LAB-ON-A-CHIP BIOSENSORS FOR THE RAPID DETECTION OF PATHOGENS IN CLINICAL AND FIELD SAMPLES

by

Christopher F. Fronczek

_____

A Dissertation Submitted to the Faculty of the

GRADUATE INTERDISCIPLINARY PROGRAM IN BIOMEDICAL ENGINEERING

In Partial Fulfillment of the Requirements

For the Degree of

DOCTOR OF PHILOSOPHY

In the Graduate College

THE UNIVERSITY OF ARIZONA

2013

THE UNIVERSITY OF ARIZONA
GRADUATE COLLEGE

As members of the Dissertation Committee, we certify that we have read the dissertation prepared by Christopher F. Fronczek

entitled Lab-on-a-chip Biosensors for the Rapid Detection of Pathogens in Clinical and Field Samples

and recommend that it be accepted as fulfilling the dissertation requirement for the Degree of Doctor of Philosophy

_____Date: 11/25/2013
Jeong-Yeol Yoon

_____Date: 11/25/2013
Terry O. Matsunaga

_____Date: 11/25/2013
Joel L. Cuello

_____Date: 11/25/2013
Sadhana Ravishankar

Final approval and acceptance of this dissertation is contingent upon the candidate's submission of the final copies of the dissertation to the Graduate College.

I hereby certify that I have read this dissertation prepared under my direction and recommend that it be accepted as fulfilling the dissertation requirement.

_____ Date: 11/25/2013
Dissertation Director: Jeong-Yeol Yoon

STATEMENT BY AUTHOR

This dissertation has been submitted in partial fulfillment of requirements for an advanced degree at the University of Arizona and is deposited in the University Library to be made available to borrowers under rules of the Library.

Brief quotations from this dissertation are allowable without special permission, provided that accurate acknowledgment of source is made. Requests for permission for extended quotation from or reproduction of this manuscript in whole or in part may be granted by the author.

SIGNED: Christopher F. Fronczek

ACKNOWLEDGEMENTS

I would like to express gratitude to my mentor and principal investigator, Dr. Jeong-Yeol Yoon, for all his support over the past few years. Besides great advice in engineering and general pearls of wisdom, he has helped me find my calling in life in the biosensors world. In addition, he has helped me to remember that there are endless possibilities in life, achieved with the proper attitude and motivation. I would also like to thank Dr. Yoon for fostering a great work environment in the biosensors laboratory.

I would also like to extend my appreciation to the members of my committee, Dr. Terry Matsunaga, Dr. Sadhana Ravishankar, and Dr. Joel Cuello, for their kind support, guidance, and advice ranging from microbiology to entrepreneurial discussions.

I wish to also thank Omid Mahdavi with the University of Arizona Micro/Nano Fabrication Center for all of his assistance and guidance involving microfabrication, particularly lithographic techniques.

I especially thank members of the biosensors laboratory for their support and comradery, both past and present, including Dr. Hyuck-Jin Kwon, Dr. Tu San Park, Christopher Stemple, Dr. Phat Tran, Dr. David You, Scott Angus, Cayla Baynes, Jessica Gamboa, Dustin Harshman, Pei-Shih Liang, Ariana Nicolini, Scott Brechbiel, Soohee Cho, Wenue Li, Katherine McCracken, Roberto Reyes, and Lily Walsh.

Finally, I would like to extend a special thanks to my family and friends who have supported and motivated me throughout my academic career.

DEDICATION

I would like to dedicate this work to my parents, who have been an inspiration to me in life. You have provided me with great wisdom over the years, and you are the reason that I have chosen this path.

TABLE OF CONTENTS

LIST OF TABLES

LIST OF FIGURES

ABSTRACT

In this dissertation, lab-on-a-chip (LOC) technology is developed for field-deployable assays and point of care diagnostics. In the United States and other developed countries, despite great efforts in time and funding for the prevention of foodborne, airborne, and bloodborne diseases, there is still an unacceptable level of common pathogens spread via food, water, and air. A few common pathogens lead to a majority of the associated costs, including prevention cost and hospitalization cost. In addition, there are an unacceptable number of deaths stemming from theses illnesses. Rapid, real-time, on-site biosensors could provide a cost effective means of prevention of the spread of these diseases. In the recent years, there has been a global push for the creation of more automated, specific, and sensitive platforms to test for such pathogens in real samples, with emphasis on assay time, simplicity, and fabrication cost. These point of care devices have applications in hospitals, agricultural farms, processing plants, and even on fields of battle. Two successful types of assays in the recent years towards point of care diagnostics are immunoassays and nucleic acid detection assays.

Immunoassays, particularly particle immunoassays, take advantage of specific antibody-antigen interactions and utilize sensitive Mie scattering by utilizing polystyrene latex sub-micron particles. Antibodies to a specific antigen target are conjugated to the surface of the particles. These assays can be easily modified for varieties of pathogen targets by simply varying the antibody type on the particle surfaces. Proper sampling techniques are crucial to maximize sensitivity, particularly when using complex samples. In addition, the protocols can be modified for sampling of airborne pathogens. Targets

range broadly in size, shape, and weight, and the assays are dependent on antigen concentration and not whole cell analysis.

Direct fluorescence detection of nucleic acid combines the specificity of targeting genomic nucleic acid with the sensitivity of fluorescence detection. In order to reduce the assay time and labor, such as those found in polymerase chain reaction (PCR) and reverse transcription polymerase chain reaction (RT-PCR), researchers have been creating LOC platforms, including lateral flow assays and microfluidic extraction chips containing magnetic beads, to measure nucleic acid content in sample. Typically, these assays focus on sample preparation, cell lysis, nucleic acid and elution, and either fluorescent or colorimetric detection.

In the first paper (Appendix A), we demonstrated a complete, field-deployable assay that utilizes a latex particle immunoassay, encased within a microfluidic chip, to detect small quantities of *Salmonella* Typhimurium in poultry fluid samples. Because the necessary reagents are pre-loaded and the test and negative control channels are fed by a single sample inlet, single pipetting of sample is possible. This assay demonstrated a 10 CFU/mL bacterial limit of detection, which is considerably lower than the standard PCR and enzyme-linked immunosorbent assay (ELISA) methods. Total assay time, including sample reading in an integrated handheld device, was 10 minutes, which was much lower than conventional methods. The portable assay can easily be fitted to point of care diagnostic applications for a variety of targets in different samples by slightly altering a few parameters, namely the antibody type. In addition, the chip and reader can be equipped to test for a variety of microbes simultaneously through multiplexing.

In the second paper (Appendix B), we fit the particle immunoassay to test for Influenza A H1N1/2009 virus and included aerosol sampling from a scaled-down mock classroom. To make the assay more field deployable, we used an iPhone for signal detection. The detection limit of the assay was 1 pg/mL (10 pg/mL using the iPhone), which is well below the limit of detection for RT-PCR. This protocol demonstrated that immunoassays can be effective in the presence of interfering dust particles and that viruses can be collected from aerosol with minimal sample preparation. This assay can be more automated to include a small air sampler placed in appropriate locations determined by information provided by the mock classroom. Primarily, the mock classroom results from the immunoassay and from RT-PCR concurrently demonstrated direction of aerosol movement with respect to two different ventillation rates.

In the third and final paper (Appendix C), we demonstrated that paper microfluidics, a newer vision of microfluidics, is a cheap and easy method to extract nucleic acid from *S.* Typhimurium in a variety of samples, including poultry packaging liquid, whole blood, and feces. This chip (made from cellulose and nitrocellulose paper), using fluorescent intercalating dye and an iPhone with reader, sensitively provides information about the total bacterial count of a sample. In addition, this protocol interfaces with PCR and provides information on whether or not extraction was successful. This assay can be modified to also provide specific information about the type of target present in samples, and the chip can be multiplexed to test a variety of samples simultaneously.

1. INTRODUCTION

1.1 Foodborne pathogens

In the United States, there are numerous outbreaks caused by bacterial infections originating from contaminated poultry, meat, produce, and water. According to the Centers for Disease Control (CDC), Nearly 1 in 6 Americans are affected by 31 common bacteria from the consumption of food products, and 128,000 are hospitalized. In addition, over 3,000 Americans die from complications due to these infections [CDC Foodborne Pathogens 2011]. Overall, these outbreaks and hospitalizations cost the food industry and medical industry nearly $10 billion per year [Health and Human Services, 2013]. Common bacterial foodborne illnesses (Table 1) [Hoffman et al. 2012], [Rangel et al. 2005] observed in the U.S. are caused by *Salmonella* species, *Campylobacter jejuni*, *Shigella* sp., *Escherichia coli*, *Listeria monocytogenes*, and *Clostridium botulinum*. These pathogens can be easily spread and can contaminate food and water due to poor sanitation. These bacterial contaminants can be isolated in meat packing facilities, food processing plants, fresh produce irrigated with contaminated water, poultry liquid in packaging, and improperly canned foods. In addition to bacterial foodborne pathogens, common viral infections, specifically norovirus and hepatitis A, are typically caused by contaminated water or by infected food handlers.

Pathology

Generally, the aforementioned foodborne illnesses are caused by contaminated irrigation and rinse water, improper food handling, or undercooking meat and poultry. Common symptoms range anywhere from nausea, vomiting and diarrhea to fever and

abdominal pain. More severe symptoms include high fever, severe gastroenteritis, weakness, and even paralysis and death. Secondary infections and complications include hemolytic uremic syndrome (HUS), reactive arthritis, meningitis, irritable bowel syndrome (IBS), and Guillain-Barré syndrome**.** In addition, renal failure is a common complication stemming from severe infections. The most susceptible populace to these complications are the immune-compromised, very young, and elderly [NDDIC 2012].

1.2 Bloodborne pathogens

Bloodborne infections due to viral and bacterial pathogens are a serious problem in the U.S. The most common modes of transmittance of these pathogens are contact with bodily fluids, blood transfusions, penetration with infected needles, and invasion into the bloodstream through open wounds. In addition, bacterial contaminants can be found in tainted platelets stored at room temperature, accounting for 1 infection out of every 2000-3000 platelet transfusions. The most common bacteria leading to bloodborne illness are *Staphylococcus epidermidis*, *Staphylococcus aureus*, *E. coli*, and *Klebsiella* sp. Viral pathogens leading to bloodborne infections include *Hepatitis* B, *Hepatitis* C, Human Immunodeficiency Virus (HIV), Ebola Virus, and West Nile Virus. Still, in underdeveloped nations, hemorrhagic fevers are quite problematic [CDC Bloodborne Pathogens 2013].

Pathology

Bloodborne pathogenic infections often arise from either infected bodily fluids entering the bloodstream or through native micro flora infecting the bloodstream. Invading pathogens travel through the blood to possible sites of infections, and certain viruses,

especially HIV, become very difficult to detect due to their retroviral genetic machinery. Symptoms of these infections vary widely and include low-grade to high-grade fever, gastroenteritis, flu-like symptoms, and weight loss. Complications often arising include cirrhosis, Acquired Immunodeficiency Syndrome (AIDS), sepsis, meningitis, and organ failure. Patients with AIDS are also more susceptible to pneumonia, intestinal disorders, and fungal infections. Patient and hospital costs due to these complications is high each year [CDC Bloodborne Sharps 2013]. It is estimated that nearly 5.6 million people working in the US healthcare industry are at a significant risk of contracting some bloodborne illness, most commonly Hepatitis A, Hepatitis C, and HIV. In addition, these common bloodborne pathogens affect over 100,000 Americans each year, leading to 20 – 30,000 deaths [CDC MMWR Occupational Exposure 2005].

1.3 Airborne pathogens

Airborne pathogens, particularly viruses from the common cold (rhinovirus) to more serious Influenzas, affect millions of Americans each year (Table 2) [CDC Tuberculosis 2011], [CDC *Streptococcus pneumoniae*, 2010]. Airborne viruses are typically transmitted in the form of aerosols, through coughing, sneezing, or talking, or in sputum, and the virus particles may remain in droplet form, termed droplet nuclei, for some time, whether in dust or liquid droplet particles. These particles may take refuge in respiratory systems or ventilation systems. Influenza A is one of the most problematic airborne viral pathogens in the U.S., and 2009/H1N1 Influenza A led to a global pandemic, including 60 million cases in the U.S., 275,000 hospitalizations, and over 10,000 deaths since 2009 [CDC H1N1 2009 2011]. Unfortunately, these viruses are highly contagious, have a fairly rapid doubling time, and are easily spread in aerosol form. Droplets larger than 100 μm in

diameter tend to settle, while those smaller than 100 μm tend to travel further in aerosol form. Tiny droplets (less than 10 μm in diameter) will remain suspended in the air for longer periods of time, and these can more easily make contact with host organism membranes for infection [CDC Seasonal Flu 2011]. These pathogens cost the healthcare industry millions of dollars per year.

Pathology

Typically, airborne viral infections occur when the proper dose of virus particles enter a mucous membrane. Common symptoms for these common viral infections include coughing, sneezing, congestion, fever, fatigue, watery eyes, headache, and sore throat, and many of these early symptoms may be mistakenly associated with allergies or simples colds. Odds of infection increase greatly in crowded spaces, humid ventilation conditions, and among the immune-compromised. More serious viral infections, including those of Influenza A, often could lead to serious secondary infections, including pneumonia, sinusitis, meningitis, and various bacterial infections. Further complicating viral infections is the virus doubling rate and the sometimes low incubation period as well as the fact that viruses are often misdiagnosed. In addition, viral infections are generally harder to treat than bacterial infections because antivirals are administered, and these medications are often cell cycle inhibitors rather than antimicrobials [Stork 2007]. While these inhibitors act to hinder and/or block the growth phase of the pathogens in host cells, they can be slow and inefficient.

Pathogen	Cases	Hospitalizations	Deaths	Total Cost
Norovirus	> 5.4 million	>14,500	>600	$ 2 billion
Salmonella Typhimurium	>1.1 million	>19,000	380	$ 3.3 billion
Campylobacter	845,000	>8,500	76	$ 1.7 billion
Toxoplasma gondii	>4,000	>4,400	>325	$ 3 billion
E. coli 0157	>75,000	2,100	>40	> $500 million

Table 1: Common foodborne pathogen statistics in the U.S. each year. These five pathogens lead to the highest number of hospitalizations and the highest total cost. Compiled from CDC, 2008-2012 reports.

Airborne Pathogen	Cases	Hospitalizations	Deaths	Total Costs
Influenza A seasonal	500,000 – 1 million	- - -	> 150	- - -
Influenza A (H1N1/2009)	> 60 million (since 2009)	> 275,000 (since 2009)	12,000 (since 2009)	$several billions
Mycobacterium tuberculosis	> 11,000	- - -	>500	> $100 million
Streptococcus pneumoniae	500,000	> 175,000	50,000	> $1 billion

Table 2: Common airborne pathogens, including viruses and bacteria, in the U.S. each year. Note that the H1N1/2009 strain statistics range from 2009-2013, from that date it was termed pandemic. Compiled from CDC, 2008-2012 reports.

1.4 Salmonellosis

Salmonellosis is a mild to severe foodbone infection resulting from *Salmonella enterica* in which the patient may be hospitalized, typically due to severe diarrhea. This

condition may arise 5-7 days after the onset of symptoms in a few patients, and these patients may then acquire secondary infections, leading to further expenses. Initially, bacteria begin to colonize in the gut and gastrointestinal tract. From there, infection spreads to intestines and then surrounding tissues. If left untreated, severe infection may occur if the infection then spreads to the bloodstream, possibly leading to sepsis and organ failure. While *S.* Typhimurium is considered foodborne and usually does not lead to sepsis, *Salmonella* Typhi may be considered waterborne and is more likely to lead to sepsis. *S.* Typhi spreads to the bloodstream more rapidly and often results in typhoid fever. Common complications arising from Salmonellosis include the onset of Reiter's syndrome and intestinal damage. For this reason, common *Salmonella* strains, especially *Salmonella* Typhimurium and *Salmonella* Enteritidis, should be some of the primary targets when detecting small amounts of foodborne bacteria in field settings [CDC Salmonellosis 2007]

1.5 Current Gold Standard Pathogen Detection Systems

Preventative care, or proactive medicine, is always preferable to reactive medicine due to the cost savings, which includes physician appointments, drug treatments, and possible hospital stays. In addition, proactive medicine reduces mortality and morbidity. However, in order to successfully provide proactive medicine, early detection of common pathogens is necessary to prevent infection and spread of disease. Therefore, since the advent of modern medicine, there has been a focus on point-of-care diagnostics in clinical settings. In addition, in more recent years, there has been a focus on field deployable assays in agricultural, food, and water industries to ensure quality of produce and reduce the risk of foodborne illness.

Culture Plating and Colony Counting

For many years, the gold standard in pathogen detection and identification has been conventional agar culture plating and colony counting. While this method is quite accurate and specific, it generally requires up to 24-36 hours. There are a variety of cell plating methods, from standard Lurial Broth (LB) agar plating for total bacterial count, spread plating, pour plating, streaking for isolation of particular bacteria, replicate organism direct agar contact plating (RODAC), MacConkey agar plating for selecting gram negative bacteria, and various agar plates incorporated with antibiotics to select either positively or negatively for specific bacterial pathogens. For the culturing of viruses, similar techniques exist that require host, generally mammalian cell lines along with various nutrients [Invitrogen Life technologies Cell Culture Basics].

Enzyme-linked Immunosorbent Assay (ELISA)

In an effort to create in-lab bench top assays that were more rapid, more user-friendly, and more sensitive, technicians began to investigate immunoassays due to the increasing knowledge of the immune system. As of the 1960s, a vast majority of these immunoassays were radioimmunoassays, in which radiolabeled antibodies were used to capture antigens. A specific antibody-antigen binding reaction would yield a signal change, but the radiolabeled reagents posed a serious health risk [Yalow and Berson 1960]. Because of this, many began to investigate the coupling of an enzyme and specific substrate for detection to bypass radioactive substances. In the early 1970s, Enzyme-Linked Immunosorbent Assay, or ELISA, was introduced, and this assay took advantage of specific antibody-antigen interactions along with colorimetric signal change for detection. The assay can use antibodies to capture antigens of interest or even antigens to capture

antibodies to interest. In the most basic indirect ELISA, a sample, possibly containing antigens of interest, is passed over a surface containing serum or bovine serum albumin (SA or BSA), and a primary antibody containing a conjugated enzyme is passed over. A secondary antibody to the primary antibody is added, and upon the addition of the specific substrate, a color change is observed if the antigen of interest was present in the sample. The higher the target concentration, the higher the color intensity. Similarly, the popular "Sandwich" ELISA contains primary antibodies pre-immobilized on a surface, and sample is then added, followed by a series of secondary antibodies and substrate. ELISA has been multiplexed into 96 well plates, and has even been introduced into microfluidic formats [Hoegger et al. 2007]. While ELISA exhibits a high degree of specificity and is quite sensitive, it is time-consuming (1-2 hours), laborious, requires several washing steps, typically requires large sample volumes, and is not portable. Furthermore, because ELISA requires several separate steps, user error is introduced, and reproducibility may be compromised.

Polymerase Chain Reaction (PCR)

With the development of ELISA, and the recognition of its deficiencies, researchers looked for more specific and sensitive methods for pathogen detection. With greater knowledge of nucleic acid, and the recognition of its supreme specificity, focus shifted to the detection of DNA and RNA. However, clinically and biologically relevant samples typically contain very small amounts of nucleic acid, making direct detection nearly impossible in many circumstances. In 1983, polymerase chain reaction (PCR) was developed to increase the amount of nucleic acid present in a sample using a process called thermal cycling. A template double-stranded DNA is broken apart, and then the

complementary strand is duplicated via polymerase chain reaction in order to make many smaller copies of a specific region of interest. Specific complementary oligonucleotide primers are used to identify the region of interest to be copied, and thermo stable DNA polymerase isolated from *Thermus aquaticus* adds nucleotides to the growing chains [Bartlet and Stirling 2003]. Cycling consists of three stages: 1) denaturation, in which the double helix is unwound into two separate strands at high temperature, 2) annealing, in which primers bind to complementary regions of interest at a lower temperature, and 3) elongation, in which nucleotides are added to the newly synthesized chains. Typically, 30 cycles will yield over a billion copies, enabling detection through fluorescent staining. In the past 30 years, PCR has been optimized to be more portable, rapid, and user-friendly in formats such as quantitative PCR (qPCR) [VanGuilder et al. 2008], hot-start PCR [Primrose et al. 2001], loop-mediated isothermal amplification PCR (LAMP) [Mori et al. 2001], and two-step PCR. PCR has been introduced into microfluidics [Sanchez-Freire et al. 2001] and has been multiplexed to test for an array of targets [Chamberlain et al. 1988]. PCR has provided excellent specificity and sensitivity and is the current gold standard for pathogen detection. However, PCR is laborious (many preparation steps), time consuming (2-6 hours), expensive (requires many reagents and specially designed primers), and not portable (meant for lab bench top analysis).

1.6 Problems with Real Samples

In addition to the drawbacks of the current gold standards for pathogen detection, clinically-relevant and real-life samples present a separate dimension of problems with detection. For example, samples such as wastewater may contain unwanted bacteria and algae which may hinder optical detection and reduce assay specificity [You et al. 2011].

In addition, complex matrices such as feces, blood, and meat or poultry wash water contain a variety of interfering components such as lipids, cells, contaminants, and proteins [Bou et al. 2006]. In addition, these samples may be turbid and viscous, making optical detection impossible. Therefore, there is a need for assay optimization in which these intrusive components are either eliminated or reduced in the form of minimal background signal-to-noise while maximizing specificity, sensitivity, and ease-of-use.

Air Sampling

When collecting samples in the form of aerosols, including bacteria such as *Mycoplasma pneumoniae* and influenza viruses, it is necessary to optimize various parameters in order to create an effective assay. Primarily, establishing air samples in ideal locations to sense detectable quantities of the pathogen of interest is crucial to this type of test. In addition, some mode of concentration should be implemented due to the typically small concentration of pathogens in aerosols. Finally, due to the abundance of dust particles and other unwanted agents, the sampling mechanism should contain some method for reducing interference from environmental particulate matter, particularly in optical detection assays. Furthermore, the vast polydispersity of dust particles adds more complication [WHO 2011, Airborne Dust], thus complicating assays.

1.7 Lab-on-a-Chip in pathogen detection

Lab-on-a-chip (LOC) is a device or platform that integrates several larger lab benchtop instruments or tests into a single, concise unit that is portable [Manz et al. 1990]. LOC generally contains microfluidic element(s) and are often used as micro total analysis systems (μTAS) due to their modularity. These devices are advantageous in that they are

compact, cheap to fabricate, require small sample volumes, are portable, and provide a high degree of process control. LOC technology has been implemented in a wide array of applications, including environmental assays [Jang et al. 2011], genomics [Jain 2002], drug discovery [Ho et al. 2013], medical diagnostics [Chin et al. 2012], and cellular analysis with cell culture [Peng et al. 2013].

Microfluidics

Microfluidics, a concept that combines fluid mechanics, physics, and micro/nanotechnology, has emerged as the chief component of LOC. Because of very small volumes (microliters, nanoliters, and even picoliters) laminar flow can be achieved in microfluidic channels, providing a very high degree of control over mixing efficiency between multiple reagents. In addition, fluid properties including viscosity, energy dissipation, and surface tension are primary factors in determining laminar flow, making capillary action in channel possible; this feature provides self-wettability and the possibility to single pipetting of sample. Because of these features, combined with the understanding of micro and nanofabrication processes, components such as vortex mixers for turbulent mixing, micropumps, microvalves, and electrodes have been implemented into microfluidic chips [Mansure et al. 2008]. Microfluidic channels and structures have been fabricated in a wide variety of materials, including polydimethylsiloxane (PDMS), poly(methyl methacrylate) (PMMA), various acrylics, polycarbonate, and glasses [Whitesides 2008], and these materials are optically clear. Hydrophobicity of these materials is also very important to flow conditions and varies per applications, and the hydrophobic nature of channels in these materials can be modified. Fabrications of chips can be cheap, depending on material, and can be accomplished through photolithography

[Kim et al. 2008], replica molding [Mustin and Stoebber 2012], micro contact printing [Watson et al. 2006], micro machining [Sugioka and Cheng 2014], and hot embossing [Becker et al. 1998]. With all of the successful work in the area of microfluidics, there remains room for improvement in integrating these devices into field-deployable biosensors.

Microfluidics in biosensors- what has been accomplished thus far

To date, microfluidic LOC devices have been incorporated in numerous types of biosensor assays, including microfluidic ELISA [Sun et al. 2010], on-chip PCR [Kopp et al. 1998], particle immunoassays [Bange et al. 2005], magnetic bead cell sorting assays [Inglis 2004], and paper microfluidic assays [Park et al. 2013]. Many of these developments have increased levels of specificity, sensitivity, ease-of-use, and portability, yet all remain incomplete in terms of total analysis. For true total analysis, a system must contain: (1) a sample preparation module with handling, (2) mixing (often microfluidic) components for reagent introduction, (3) capture region in which the pathogen or analyte is detected, (4) detection region in which a signal is produced to show the presence of the detected specimen, (5) and a user interface in which the signal is transferred to some readable format. For portability and ease-of-use, these components should be contained in some casing, and operator labor should be minimized to reduce the possibility of user error.

2. OVERVIEW OF DISSERTATION

This dissertation encompasses three separate biosensor publications that incorporate microfluidic LOC technology towards true field-deployable, point of care diagnostics in a variety of samples. Potential applications include; 1) pre-processing quality control checks at meat and poultry packaging facilities; 2) environmental water quality monitoring; 3) clinical testing of bodily samples; 4) quality control at produce packaging houses; 5) testing of air samples in clinical settings near air vents to help reduce the spread of contagious pathogens; and 6) monitoring or air in food processing plants to increase product shelf life. Overall, these assays have the potential to prevent the outbreak of serious diseases and increase consumer health and safety.

2.1 Optical Biosensors for Field-deployable and Point-of-care Diagnostics

Field-Deployable/Point of Care Diagnostics

Currently, there is much emphasis on microfluidic platforms for field-deployable and point of care diagnostics. This provides the flexibility of testing for multiple target pathogens in multiple samples in different settings. Furthermore, on-site testing allows for quick results and can therefore be crucial in preventing disease outbreaks or even alleviating symptoms of disease before they become more severe. Recently, research has focused on providing cheaper and more portable solutions for point of care testing in order to make field-deployable testing more possible in remote areas. For this type of testing, devices must meet the following criteria: (1) allow for minimal sample preparation and pretreatment, (2) allow for minimal sample input while minimizing limit of detection, (3) be user friendly and be automated, (4) be portable, (5) be cheap to manufacture, and (6)

provide easy to interpret data to provide direct information regarding the analyte of interest [Linder 2007].

2.1 a Particle Immunoagglutination Assay

Particle immunoassays provide the good antibody-antigen binding specificity found in ELISA while greatly reducing total assay time. Because of this specificity, assays can be accomplished in a wide variety of complex samples containing interfering proteins, cells, and lipids [Heinze et al. 2009]. The particle immunoassay based on latex agglutination assays has been established to detect small amounts of pathogens present in samples such as blood, saliva, and urine and has been optimized to eliminate washing steps. Polystyrene latex sub-micron particles are conjugated with specific antibodies, and pathogen suspensions are mixed with particle suspensions. Upon introduction of antigens to specific antibodies of interest, binding reactions occur, termed immunoagglutination. Agglutinants in high concentrations can be visualized because they fall out of solution, but this detection method is impractical since relevant samples often contain small quantities of pathogen. To optimize sensitivity, light scattering techniques have been implemented [Yoon 2008]. While ELISA kits have been optimized for increased sensitivity, forward light scattering detection implemented in particle immunoassays provides better sensitivity.

Light Scattering

It has been shown that measuring light scattering across agglutinated particles provides supreme sensitivity to the particle immunoassay [Heinze and Yoon 2011], [You et al. 2011], [Song et al. 2011], [Stemple et al. 2012]. In forward and back light scattering

applications, incident light at a fixed wavelength is focused on the immune reaction area, and a detector, typically a CCD, is used to measure light scattering across the reaction. Agglutinants form doublets and triplets from singlets. The amount of target antigen present in the sample is proportional to the amount of immunoagglutination and therefore proportional to the scattering signal intensity measured. Analyzing this scattering produces log-linear curves, and the linear regions provide the most useful information in back-calculating an antigen concentration from a signal output. Light scattering can be divided into two categories: elastic and inelastic. In elastic light scattering, there is no significant shift in the amount of energy transferred when passing particulate matter. Elastic light scattering can be subdivided into Raleigh and Mie scatter. Classification of light scatter depends on the ratio of incident light (λ) to the particle diameter (d). Raleigh scattering can be modeled as [S. Prahl]:

$$\frac{I}{I_0} = \frac{1+\cos^2\theta}{2R^2}\left(\frac{2\pi}{\lambda}\right)^4\left(\frac{n^2-1}{n^2+2}\right)^2\left(\frac{d}{2}\right)^6$$

In this model, I = signal scattering intensity, Io = incident light intensity, R = distance from particle to detector, θ = scattering angle, n = refractive index of particles, λ = wavelength of incident light, and d = particle diameter. While this complex model contains many components, when R, λ, and θ are fixed and optimized, d becomes dominant in determining scattering intensity. Therefore, optimizing d will enable a good increase in scattering intensity with particle growth. With this information, one can optimize Mie scatter, in which particle diameter is greater than or equal to the wavelength of incident light. This factor, as well as detection angle, dominates in Mie scattering, which can be modeled as [Kerker 1969]:

$$i_1 = \left| \sum_{n=1}^{\infty} \frac{2n+1}{n(n+1)} (a_n \pi_n \cos\theta + b_n \tau_n \cos\theta) \right|^2$$

$$i_2 = \left| \sum_{n=1}^{\infty} \frac{2n+1}{n(n+1)} (a_n \tau_n \cos\theta + b_n \pi_n \cos\theta) \right|^2$$

where i_1 and i_2 are complex scattering amplitudes heavily dependent upon refractive index and scattering angle. Utilizing Mie scatter phenomenon allows for optimization of d and θ, maximizing sensitivity and helping in part to reduce background noise from sample. The use of polyclonal antibodies provides target flexibility due to multiple epitope binding sites, eliminating the need for purely lysed or intact cells. Therefore, antigens from dead cells can be detected. In addition, the use of polyclonal antibodies fosters the formation of triplets during the reaction. These two factors work to maximize scattering intensity, helping to reduce the detection limit of the assay.

Incorporating microfluidics into the particle immunoassay provides several advantages. First, laminar flow provides good mixing between the sample, pathogens, and reagents. Second, high surface area to volume ratio increases the reaction rate, allowing for decreased assay time. Third, small dimensions allow for small sample and reagent volumes, thereby reducing the cost of materials. Fourth, automated fluid handling, especially through capillary action, reduces user handling, thereby minimizing operator error and therefore increasing reproducibility. Finally, the microenvironment causes minimal vertical layering of particles and reduces scattering gradients. All of these factors contribute to sensitivity, assay reliability, and lower manufacturing cost [Wu et al. 2009].

While laminar flow is advantageous because it provides good control over mixing, it is problematic due to the fact that the particles (around 1 μm in diameter) do not passively diffuse well. This obstacle is largely overcome by using highly carboxylated polystyrene latex particles, but scattering signal stability often remains compromised. This instability may be due to either lack of particle mixing or even particle non-specific interactions. To further increase assay sensitivity, surfactant such as Tween 80 is included to break apart non-specific agglutinants at low concentrations.

2.1 b Direct Fluorescent Detection of Nucleic Acid from Pathogens

While the particle immunoassay has revolutionized the field of biosensors, the gold standard for pathogen identification remains nucleic acid detection, chiefly achieved through PCR and RT-PCR. However, these processes include hours of labor, including sample preparation, thermal cycling for amplification, and detection of amplicon product. To create a field-deployable assay towards point of care diagnostics, total protocol time should be greatly reduced, and testing should be accomplished on site without bulky equipment. Therefore, an alternative option is to directly detect genomic nucleic acid from targets in samples. However, this approach is difficult because of the very tiny yields of genomic nucleic acid, possibly as low as the picogram scale [You et al. 2012]. Therefore, an extremely sensitive reagent is required. Intercalating dyes, fluorescent dyes that typically bind to the backbone grooves of double stranded DNA and intertwine between the strands, have been used for years in such applications. Upon intercalation, the dyes fluoresce, and the resulting fluorescence is measured. Recently, more sensitive dyes with higher extinction coefficients have been created. For example, Invitrogen Life Technologies marketed PicoGreen dye, which forms a third bond with backbone

phosphoryl groups. This highly sensitive dye can detect as little as 25 pg/mL of double stranded DNA, even in the presence of single stranded DNA and RNA. Upon intercalation, there is > 1000 fold increase in the fluorescence signal [Dragan et al. 2010]. With increasing DNA content, there is increasing fluorescence signal.

Extraction and Elution of Nucleic Acid

In order to incorporate fluorescence detection of nucleic acid into field-deployable biosensors, the genetic material must first be extracted from microbes. However, existing methods for nucleic acid extraction and purification involve laborious steps. Also, due to the fact that many of these protocols include organic solvents (solvent extraction), centrifugation and washing steps are necessary, requiring bulky laboratory equipment. In addition, many preferred methods take 30 minutes to an hour [Singh et al. 2002]. In order to maximize nucleic acid yield, good care must be taken to remove contaminants. Furthermore, all PCR inhibitors should be removed or inactivated. To reduce sample preparation time and user error, organic solvents and centrifugation should be eliminated from the protocol. A popular alternative to solvent extraction is solid phase extraction, in which nucleic acid is either physically captured for purification or passed through some membrane for capture. For example, silica beads have been used to either bind or filter DNA [Cady et al. 2003]. Companies such as Qiagen (Invitrogen Life Technologies, Grand Island, NY, USA) have developed chromatography columns for effective extraction and purification, but many of these protocols still contain centrifugation steps.

Microfluidics appears as a promising approach for efficient genomic nucleic acid extraction due to the small sample volume requirements and good control over mixing provided by laminar flow. In addition, microfluidic chips can be equipped with a variety

of filters for sample separation as well as valves for the injection of various reagents. Overall, microfluidics could allow for cheap and quick on site nucleic acid extraction from clinical and field samples, and fluorescence detection could be included for a total analysis system.

Paper microfluidics is an emerging technology applicable in a variety of biosensors applications [Martinez et al. 2008]. Microfluidic channels are patterned on paper using a modified lithography technique, rendering a hydrophilic patterned region surrounded by a very hydrophobic exterior. This technique is a good alternative to traditional microfluidics because paper fibers allow for filtering, flow is driven by capillary action, and manufacturing cost is cheap. Furthermore, channel width can be modified to dictate flow speed and distance since channels are 2-dimensional. These paper chips have potential applications in field-deployable point of care diagnostics and can serve as a platform for numerous assays [Park et al. 2013]. Due to their excellent filtration properties, paper microfluidics is an attractive approach to nucleic acid extraction from pathogens in complex samples. First, pathogens and small components can be filtered near the sample inlet of the chip, and following a simple lysis step, nucleic acid can be filtered from cell fragments and other interfering materials. To quantify extraction efficiency, intercalating dye may be loaded at the appropriate sites along the channel, and fluorescence can be quantified. Chips can be designed for a variety of sample and pathogen types and can be modified for dip tests to allow for easy sample loading.

3. CONCLUSIONS

We have developed rapid, sensitive, and field deployable assays that are easy to use, contain disposable components, and are functional in a variety of relevant field and clinical samples. While we have made great strides, particularly in the areas of sensitivity and assay time, more improvements must be made in order to create systems that will revolutionize the field of point-of care diagnostics. Primarily, detection limit, particularly in terms of nucleic acid detection from bacterial cells, can be lowered. While these assays are capable of detecting miniscule quantities of pathogen well below the infectious doses of most common bacteria, our systems must fall in line with industrial and regulatory standards, which are increasingly becoming more stringent.

Our assays should also be multiplexed to test for a wide variety of infectious agents in complex samples. While multiplexing microfluidic channels in the reaction platforms is fairly simple, detection becomes more complex. For example, an array of laser diodes and highly sensitive avalanche photodiodes (APDs) would need to be implemented into our particle immunoassay handheld device, which would require either more space or miniaturization, thus increasing the cost of fabrication. Furthermore, smart phone detection would become more challenging and would either require further application programming or larger readers. Besides testing for multiple types of bacteria or viruses, multiplexing could provide the feasibility of increasing reproducibility or even provide for attempting several different tests for a single pathogen.

In addition to sensitivity and multiplexing optimizations, our assays, particularly, our aerosol microfluidic immunosensor, should be more portable and automated. Ideally, the

sampler would be smaller and directly attached to the microfluidic chip, which would be encased in a reader that is adaptable to a smart phone. With this optimization, one could carry the device to testing regions of interest and sample the air in real-time. Alternatively, the sampler and microfluidic components could be stationed at locations of risk, and an automated system would periodically check the air for known pathogens or reagents. The smart phone could be replaced with a simple LED and photodiode array, and Blue tooth technology could be implemented to provide information to a remote phone or computer.

Finally, the paper microfluidic apparatus for testing pathogenic nucleic acids can be equipped with an element of specificity. Currently, this assay only provides total bacterial concentration in complex sample, and not specifically what is present in the sample. If the paper chip is multiplexed, the assay may be functionalized to either positively or negatively select for certain types of cells or nucleic acid, possibly based on size, weight, or some surface marker.

4. FUTURE DIRECTIONS

The single pipetting particle immunoassay is already near completion necessary for marketability. Besides a perfectly standardized negative control, the microfluidic chip can be multiplexed to test for multiple pathogens or even the same pathogen in multiple samples. With the dual negative control-test channel layout, true single pipetting of sample can still be achieved through the use of a specially designed syringe that can load multiple wells simultaneously. Such a solution would be cheap to produce while increasing the market value of the particle immunoassay apparatus. While this assay is very specific,

there is potential for cross reactivity between common pathogenic ancestors, such as *E. coli* and *Salmonella*. While this problem can be overcome by careful testing of the anti-*Salmonella* Immunoglobulin G, cross reactivity is an issue inherent to polyclonal antibodies. In addition, for this assay to be effective in testing larger quantities of water, such as irrigation water, some concentration mechanism must be implemented due to the fact that there are typically very small amounts of pathogen present in very large volumes of the water.

While the aerosol microfluidic immunosensor provides a sensitive and portable technique to accurately detect the H1N1 virus despite the presence of interfering dust particles, this protocol can be further developed to optimize automation. For example, the current method requires that the filter be removed from the air sampler and washed in PBS solution in order to obtain fluid to load for the particle immunoassay. In order to bridge the two components of this assay, continuous sampling can be established, and collected aerosol can be automatically driven to the immune reaction area in the chip. This automation would allow for assay mounting in public areas. In addition, the air sampler can be miniaturized and equipped with fan and air bubbler to drive fluidic force for immune reaction in a portable, handheld device. This protocol could also interface with a smart phone and be used for on-site air testing for various chemical and biological agents. While this assay is very sensitive, very tine quantities of pathogens are present in aerosol samples. Thus, an automated target concentration step must be implemented in the protocol for this assay to become marketable.

The paper microfluidic micro Total Analysis System (μTAS) device for fluorescent nucleic acid detection may be modified to include an element of specificity. While the

chip currently provides information on total bacterial concentration in a sample as well as nucleic acid extraction efficiency, the ability to provide data on specifically what type of pathogen(s) is in the sample will effectively make this system a point of care μTAS apparatus. This task is not trivial due to the lack of efficiency of colorimetric oligonucleotide probes on the market. However, the microfluidic channels themselves may be modified to either sort pathogens based on some physical property or sort genomes based on some physical property. This sorting, or positive selection, can be accomplished through chip multiplexing.

5. REFERENCES

Antibacterials, Antifungals, and Antivirals. From, the Clinical Basis of Medical Toxicology, by Christine M. Stork. McGraw-Hill Professional. December 2007. Pg. 817-832.

Bange, A., Halsall, H.B., Heineman, W.R. Microfluidic immunosensor systems. Biosesnsors and Bioelectronics, 2005; 20(12): 2488–2503.

Bartlet, J.M.S., Stirling, D. A Short History of the Polymerase chain Reaction. PCR Protocols 2003; 226: 3-6.

Becker, H., Dietz, W., Dannberg, P. Microfluidic manifolds by polymer hot embossing for μtas applications. Proceedings of Micro Total Analysis Systems, 1998; 253-256.

Bou, R., Grimpa, S., Guardiola, F., Barroeta, A.C., Codony, R. Effects of various fat sources, alpha-tocopheryl acetate, and ascorbic acid supplements on fatty acid composition and alpha-tocopherol content in raw and vacuum-packed, cooked dark chicken meat. Poultry Science, 2006; 85: 1472–1481.

Cady, N.C., Stelick, S., Batt, C.A. Nucleic acid purification using microfabricated silicon structures. Journal of Biomechanical Engineering, 2003; 121(1): 22-27.

CDC Bloodborne Pathogen Statistics, 2013. http://www.cdc.gov/bloodsafety/bbp/diseases_organisms.html.

CDC Foodborne Illness Statistics, 2011. http://www.cdc.gov/foodborneburden/2011-foodborne-stimates.html.

CDC MMWR- Updated U.S. Public Health Service Guidelines for the Management of Occupational Exposures to HIV and Recommendations for Postexposure Prophylaxis, 2013. http://www.cdc.gov/mmwr/preview/mmwrhtml/rr5409a1.htm#APPENDIX.

CDC Salmonellosis Statistics, 2012. http://www.cdc.gov/nczved/divisions/dfbmd/diseases/salmonellosis/.

CDC Seasonal Influenza (Flu) in the Workplace, 2012. http://www.cdc.gov/niosh/topics/flu/transmission.html.

CDC Sharp Objects-Bloodborne Pathogen Statistics, 2013. http://www.cdc.gov/niosh/stopsticks/bloodborne.html.

CDC *Streptococcus pneumoniae* Staistics, 2010. http://www.cdc.gov/vaccines/pubs/pinkbook/downloads/pneumo.pdf.

CDC Statistics H1N1 2009, 2011. http://www.cdc.gov/h1n1flu/estimates_2009_h1n1.htm.

CDC Tuberculosis Statistics, 2012. http://www.cdc.gov/tb/statistics/reports/2012/default.htm.

Cell Culture Basics. Invitrogen Life Technologies, Accessed November 2013. http://www.invitrogen.com/cellculturebasics.

Chin, C.D., Linder, V., Sia, S.K. Commercialization of microfluidic point-of-care diagnostic devices. Lab on a Chip 2012; 12(12): 2118-2134.

Chamberlain, J.S., Gibbs, R.A., Ranier, J.E., Nguyen, P.N., Caskey, C.T. (1988). Deletion screening of the Duchenne muscular dystrophy locus via multiplex DNA amplification. Nucleic Acids Research 1988; 16(23): 11141–11156.

Dragan, A.I., Casas-Finet, J.R., Bishop, E.S., Strouse, R.J., Schenerman, M.A., Geddes, C.D. Characterization of PicoGreen Interaction with dsDNA and the Origin of Its Fluorescence Enhancement upon Binding. Biophysics, 2010; 99(9): 3010–3019.

Jang, A., Zou, Z., Lee, K.K., Ahn, C.H., Bishop, P.L. State-of-the-art lab chip sensors for environmental water monitoring. Measurement Science and Technology 2011; 22(3).

Heinze, B.C., Song, J-Y, Lee, C-H, Najam, A., and Yoon, J-YMicrofluidic Immunosensor for Rapid and Sensitive Detection of Bovine Viral Diarrhea Virus. Sensors and Actuators B: Chemical 2009; 138(2): 491-496.

Heinze, B.C., Yoon, J-Y. Nanoparticle Immunoagglutination Rayleigh Scatter Assay to Complement Microparticle Immunoagglutination Mie Scatter Assay in a Microfluidic Device. Colloids and Surfaces B: Biointerfaces 2011; 85(2): 168-173.

Ho, C.T., Lin, R.Z., Chen, R.J., Chin, C.K., Gong, S.E., Chang, H.Y., Peng, H.L., Hsu, L., Yew, T.R., Chang, S.F., Liu, C.H. Liver-cell patterning lab chip: mimicking the morphology of liver lobule tissue. Lab Chip 2013; 18: 2578-3587.

Hoegger, D., Morier, P., Vollet, C., Heini, D., Reymond, F., Rossier, J.S. Disposable Microfluidic ELISA for the Determination of Folic Acid Content in Food Products. Anal Bioanal Chem 2007; 387: 267-275.

Hoffmann, S., Batz, M.B., Morris, J.R., Glenn, J. Annual Cost of Illness and Quality-Adjusted Life Year Losses in the United States Due to 14 Foodborne Pathogens. Journal of food Protection 2012; 7: 1292-1302.

Inglis, D.W. Continuous microfluidic immunomagnetic cell separation. Applied Physics Letters, 2004; 85(21): 5093-5095.

Jain, K.K. Post-genomic applications of lab-on-a-chip and microarrays. Pharma biotech 2002; 20(5): 184-185.

Kerker, M. The Scattering of Light and Other Electromagnetic Radiation, Academic, New York, 1969.

Kim, P., Kwon, K.W., Park, M.C., Lee, S.H., Kim, S.M., Suh, K.Y. Soft Lithography for Microfluidics: a Review. Biochip Journal, 2008; 2(11): 1-11.

Linder, V. Microfluidics at the crossroad with point-of-care diagnostics. Analyst 2007; 132: 1186-1192.

Mansur, E.K., YE Minxing, Wang, Y., Dai, Y. A State-of-the-Art Review of Mixing in Microfluidic Mixers. Chinese Journal of Chemical Engineering 2008; 16(4): 503-516.

Manz, A., Graber, N., Widmer, H.M. Miniaturized total Chemical Analysis systems: A Novel Concept for Chemical Sensing. Sensors and Actuators, B 1990; 1: 244-248.

Martinez, A.W., Phillips, S.T., Wiley, B.J., Gupta, M., Whitesides, G.M. FLASH: A rapid method for prototyping paper-based microfluidic devices. Lab on a chip, 2008; 8: 2146–2150.

Mori, Y., Nagamine, K., Tomita, N., Notomi, T. Detection of loop-mediated isothermal amplification reaction by turbidity derived from magnesium pyrophosphate formation. Biochemical and Biophysical Research Communications 2001; 289: 150-154.

Mustin, B., Stoeber, B. Low cost integration of 3D-electrode structures into microfluidic devices by replica molding. Lab Chip, 2012; 2(22):4702-4708.

National Digestive Disease Information Clearinghouse (NDDIC), Foodborne Illnesses, 2012.http://digestive.niddk.nih.gov/ddiseases/pubs/bacteria/.

Park, T.S., Li, W., McCracken, K.E., and Yoon, J-Y. Smartphone quantifies *Salmonella* from paper microfluidics. Lab on a Chip, 2013; 13: 4832-4840.

Peng, C-C, Liao, W-H, Chen, Y-H, Wu, C-Y, Tung, Y-C. A microfluidic cell culture array with various oxygen tensions. Lab on a Chip 2013; 13: 3239-3245.

Prahl, S. Mie Scattering Calculator., 2007. Available: http://omlc.ogi.edu/calc/mie_calc.html.

Primrose, S.B., Richard, M,. Twyman, R.W. Principles of Gene Manipulation. 2001. Wiley- Blackwell, pg. 23.

Rangel, J.M., Sparling, P.H., Crowe, C., Griffin, P.M., Swerdlow, D.L. Epidemiology of *Escherichia coli* O157:H7 Outbreaks, United States, 1982–2002. Emerging Infectious Diseases 2005; 11(4).

Sanchez-Freire, V., Ebert, A.D., Kalisky, T., Quake, S.R., Wu, J.C. Microfluidic single-cell real-time PCR for comparative analysis of gene expression patterns. Nature

Protocols 2012; 7(5): 829-838.

Singh, R.P., Nie, X., Singh, M., Coffin, R., Duplessis, P. Sodium sulphite inhibition of potato and cherry polyphenolics in nucleic acid extraction for virus detection by RT-PCR. Journal of Virological Methods, 2002; 99(1-2): 123-31.

S. Prahl, Mie scattering calculator, Oregon Medical Laser Center, Beaverton, 2007. http://omlc.ogi.edu/calc/mie_calc.html. Accessed 15 Oct. 2010.

Sugioka, K., Cheng, Y. Femtosecond Laser 3D Micromachining for Microfluidic and Optofluidic ApplicationsEngineering, 2014; (1): 1.

Sun, S., Yang, M., Kostov, Y., Rasooly, A. ELISA-LOC: lab-on-a-chip for enzyme-linked immunodetection. Lab on a Chip, 2010; 10: 2093–2100.

Watson, M.W., Abdelgawad, M., Ye, G., Yonson, N., Trottier, J., Wheeler, A.R. Microcontact printing-based fabrication of digital microfluidic devices. Anal Chem., 2006; 78(22):7877-7885.

US Department of Health and Human Services, National Digestive Diseases Information Clearinghouse, 2013. http://digestive.niddk.nih.gov/ddiseases/pubs/bacteria/.

VanGuilder, H.D., Vrana, K.E., Freeman, W.M. Twenty-five years of quantitative PCR for gene expression analysis. Biotechniques 2008; 44(5): 629-626.

Whitesides, G.M. The origins and the future of microfluidics. Nature, 2006; 442: 368-373.

WHO (World Health Organization), 1999. Hazard Prevention and Control in the Work Environment: Airborne Dust (WHO/SDE/OEH/99.14). WHO: Geneva, pp. 1-15.

Wu, S., Zhong, Z., Wang, D., Li, M., Qing, Y., Dai, N., Li, Z. Gold nanoparticle-labeled detection antibodies for use in an enhanced electrochemical immunoassay of hepatitis B surface antigen in human serum. Microchim. Acta, 2009; 166: 269-275.

Yalow, R.S., Berson, S.A. Immunoassay of Endogenous Plasma Insulin in Man. The American Society for Clinical Investigation 1960; 39(7): 1157-1175.

Yoon, J-Y. Latex Immunoagglutination Assay in Lab-on-a-Chip. Biological Engineering (presently Biological Engineering Transactions), 2008; 1(1): 79-94.

You, D.J., Geshell, K.J., Yoon, J-Y. Direct and Sensitive Detection of Foodborne Pathogens within Fresh Produce Samples Using a Field-Deployable Handheld Device. Biosensors and Bioelectronics 2011; 28(1): 399-406.

You, D.J., Yoon, J-Y. Droplet Centrifugation, Droplet DNA Extraction, and Rapid Droplet Thermocycling for Simpler and Faster PCR Assay Using Wire-Guided Manipulations. Journal of Biological Engineering, 2012; 6: 15.

APPENDIX A

SINGLE-PIPETTING MICROFLUIDIC ASSAY DEVICE FOR RAPID DETECTION OF *SALMONELLA* FROM POULTRY PACKAGE

Christopher F.Fronczek [a], David J. You [b], Jeong-Yeol Yoon [a,b,*]

a Biomedical Engineering Graduate Interdisciplinary Program, The University of Arizona, Tucson, AZ85721-0038,USA

b Department of Agricultural and Biosystems Engineering, The University of Arizona,Tucson,AZ85721-0038,USAPublished in Biosensors and Bioelectronics 40 (2013) 342–349

Received 13 April 2012; received in revised form 3 July 2012; accepted 13 July 2012; available online 10 August 2012

Abstract

A direct, sensitive, near-real-time, handheld optical immunoassay device was developed to detect *Salmonella* Typhimurium in the naturally occurring liquid from fresh poultry packages (hereafter ‘‘chicken matrix’’), with just single pipetting of sample (i.e., no filtration, culturing and/or isolation, thus reducing the assay time and the error associated with them). Carboxylated, polystyrene microparticles were covalently conjugated with anti-Salmonella, and the immunoagglutination due to the presence of Salmonella was detected by reading the Mie scatter signals from the microfluidic channels using a handheld device. The presence of chicken matrix did not affect the light scatter signal, since the optical parameters (particle size d, wavelength of incident light l and scatter angle y) were optimized to minimize the effect of sample matrix (animal tissues and blood proteins, etc.). The sample was loaded into a microfluidic chip that was split into two channels, one pre-loaded with vacuum-dried, antibody-conjugated particles and the other with vacuum-dried, bovine serum albumin-conjugated particles. This eliminated the need for a separate negative control, effectively minimizing chip-to-chip and sample-to-sample variations. Particles and the sample were diffused in-channel through chemical agitation by Tween 80, also vacuum-dried within the microchannels. Sequential mixing of the sample to the reagents under a strict laminar flow condition synergistically improved the reproducibility and linearity of the assay. In addition, dried particles were shown to successfully detect lower Salmonella concentrations for up to 8 weeks. The handheld device contains simplified circuitry eliminating unnecessary adjustment stages, providing a stable signal, thus maximizing sensitivity. Total assay time was 10 min, and the detection limit 10 CFU ml^{-1} was observed in all matrices, demonstrating the suitability of this device

for field assays.

1. Introduction

The United States Centers for Disease Control (CDC) has reported that as of 2011, foodborne illnesses affect 48 million Americans, and Salmonella leads to the highest number of hospitalizations (CDC, 2011). Currently, conventional methods for detection of food-borne pathogens, including standard cell colony counting, enzyme-linked immunosorbent assay (ELISA), and polymerase chain reaction (PCR) (Munster et al., 2005; Mandal et al., 2011), are labor-intensive, time-consuming, and require large numbers of cell culture (Mairhofer et al., 2009). Microfluidics appears as good approach for immunoassays, particularly because the major mechanism of mixing is diffusion, and the flow is strictly laminar, allowing for controllable and highly reproducible mixing between sample and reagents in a microchannel (Han et al., 2007). This reduces the sample-to-sample variation and the standard errors of measurement, effectively improving detection limit. Our laboratory has particularly studied the demonstration of particle immunoagglutination in microfluidics and its optical detection, resulting in good sensitivity and reproducibility (Song et al., 2011; Han et al., 2008; Lucas et al., 2007a, b). In an effort to produce a more portable, rapid system for the detection of pathogens in food sample and/or its rinse water, our laboratory has recently developed a highly-sensitive microfluidic device based on Mie scattering particle immunoagglutination assay for the detection of Escherichia coli from lettuce samples (You et al., 2011). While this device features a low detection limit (down to 10 CFU mL^{-1}) and requires little sample

preparation, it requires liquid particle conjugates, and thus refrigeration, which is inappropriate for field assays. In addition, the 50% infectious dose (ID_{50}) of typical Salmonella strains is 1000 times lower than that of typical *E. coli* strains (Lawly et al., 2008),thus very low detection limit is needed in detecting *Salmonella*.

While much progress has been made in rapid optical biosensors, there is a need to detect common food pathogens with minimal sample preparation, particularly in a dirty matrix, with the goal of maximizing sensitivity. Bioluminescence detection of *E. coli* has been demonstrated to yield a detection limit of 32 CFU mL^{-1}, but the total assay time is 20 min (Guan et al., 2010). *Salmonella* was detected using a novel antibody-coated cantilever device, but the detection limit was reported to be 10^3 CFU mL^{-1} with an assay time of 40 min (Ricciardi et al., 2010). More sensitive methods, such as PCR, have detected *Salmonella* at 60 CFU mL^{-1} (Li et al., 2010a, b), but the total time including sample preparation exceeded 3 h. With an ultimate goal of developing a fully automated detection system to eliminate human error and contamination (Mandal et al., 2011), pre-loading a testing apparatus with conjugated particles would be beneficial in facilitating field-testing. Vacuum drying of particles may be a simple approach for pre-loading, and this may provide a more viable option for long-term storage while allowing for single-pipette loading of sample. When introducing the sample to pre-loaded, dried particles, diffusion should mimic the aforementioned model to ensure adequate resuspension and mixing of particles with target pathogen (Han et al., 2007). In analyzing matrices more complex than rinse water for vegetables or ground plant samples (You et al., 2011), such as animal tissues, it is very important to consider sample content. Chicken carcass contains blood proteins, lipids, fatty acids, and many nutrients, creating favorable conditions for bacterial growth

(Zhao et al., 2009; Bou et al., 2006). Therefore, if bacteria are introduced into fresh chicken packaging during processing, there is a potential for more widespread contamination. In addition, this complicated sample matrix may adversely affect the optimized Mie scatter detection of particle immunoagglutination assay.

In this study, we have developed a particle immunoagglutination assay with Mie scattering detection of *Salmonella* Typhimurium in water from poultry packaging, or ‘‘chicken matrices,’’ enclosed within a handheld, microfluidic device. Unlike in previous studies, this system is optimized for complex animal matrices containing animal tissues and blood proteins. This sensitive device allows for single pipetting of complex chicken matrix sample, meaning all reagents are pre-loaded (vacuum-dried) into a microfluidic chip, and sample does not require filtration, culturing and/or isolation. This system involves in-channel diffusion of antibody-conjugated particles leading to reproducible mixing with the sample. This diffusion is assisted by chemical agitation using Tween 80, also vacuum-dried within the microchannels. The single sample inlet and dual channels allow for collecting the target and negative control signals using the same sample within the same micro-fluidic chip, thus eliminating chip-to-chip and sample-to-sample variations. Immunoagglutination is quantified in parallel through laser diodes, a differential operational amplifier, and avalanche photodiodes (APD). We also aim to develop a new, simplified circuit design for APD to eliminate the signal drift due to noise and self-heating, thereby resulting in more reliable results. The system is designed to sensitively quantify *Salmonella* Typhimurium antigen with ease of use and short assay time, i.e., suitable for field assays.

2. Materials and method

2.1. *Salmonella* Typhimurium preparation

The *Salmonella* Typhimurium Z005 strain (ZeptoMetrix, Buffalo, NY, USA) was cultured in 25 mg mL^{-1} brain heart infusion broth (Remel, Lenexa, KS, USA). It was incubated for 12 h at 37 1C with the final concentration of 8.6×10^8 CFU mL^{-1}. 10 mL brain heart infusion broth was used for culturing. This bacterial culture (assumed 10^9 CFU mL^{-1}) was used to make serial dilutions in 50 mM pH 7.4 phosphate buffered saline (PBS).

2.2. Chicken sample preparation

In order to simplify field-testing, laborious preparation processing steps, such as grinding, should be eliminated from a protocol. Poultry samples should be washed to collect sample matrix, or liquids should be collected straight from packaging material. Fresh chicken thighs were purchased from local stores. The fresh liquid was extracted from the packaging with no further processing (Fig. 1A). The extracted liquid samples were confirmed to be negative for K005 using standard cell plating techniques. The raw samples were then used to make 10% and 1% dilutions in 50 mM PBS. Hereafter, the testing matrices will be termed PBS, 1%, and 10% chicken matrix. 2 mL aliquots of these matrix dilutions were placed in centrifuge tubes and refrigerated until use, and they were monitored daily and never used after 4 weeks. For testing, the sample matrices were spiked with the serially diluted *S*. Typhimurium to the appropriate ratios, ensuring that the sample matrix was not further diluted. The spiked samples were placed in 2 mL centrifuge tubes at room temperature during testing.

2.3. Handheld optical detection system

Fig. 1C depicts the sample casing portion of the handheld device, including a platform for the microfluidic/two-well chip, avalanche photodiodes (APDs) set at 451 above the test chip, and 650 nm laser diode light sources set under the test chip. This device incorporates all optimized parameters (d, l, and y), obtained from a series of Mie scatter simulation and spectrometric analysis of sample matrices. The case of the whole testing apparatus was designed using SolidWorks 2010 (SolidWorks Corp., Concord, MA, USA). The casing was printed in acrylonitrile-butadiene-styrene (ABS) using a Dimension 1200ES 3D printer (Stratasys, Inc., Eden Prairie, MN, USA). The APDs were kept in dark conditions during testing. To achieve light scattering of the immunoagglutinated polystyrene latex particles, two 3 mm laser diodes (7 mm collimating lenses) (Lasers4U, Co. Walnut Creek, CA, USA) were placed directly below the ‘‘viewing’’ areas of the microfluidic chip. Two UV–vis silicon APDs (Edmund Optics, Barrington, NJ, USA) were positioned above the viewing areas of the chip to detect the scattering intensity, and the differential voltage from the APDs was amplified through a differential operational amplifier (TL-082). This is a JFET (junction field effect transistor) operation amplifier designed to work with low input current (i.e., high imput impedance). The gain was set to 200,000 with single-stage differential amplification, thus it required no zero adjustment stage. In You et al. (2011), six-stage amplifications with multiple zero-adjustment stages were used. In addition, a first-order low pass filter with a cutoff frequency of 160 Hz was also added. The final output signals were read through a Rigol D21052E digital oscilloscope (Rigol Technologies, Inc., Oakwood Village, OH, USA). This simplified, yet improved version of a circuit was designed to reduce the noise and measurement-to-

measurement variation.

2.4. Microfluidic chip and microparticle preparation

The microfluidic chips were fabricated in polycarbonate using micro non-circular milling equipment. Briefly, a Roland MDX 540A (Roland DG Corp., Irvine, CA, USA)

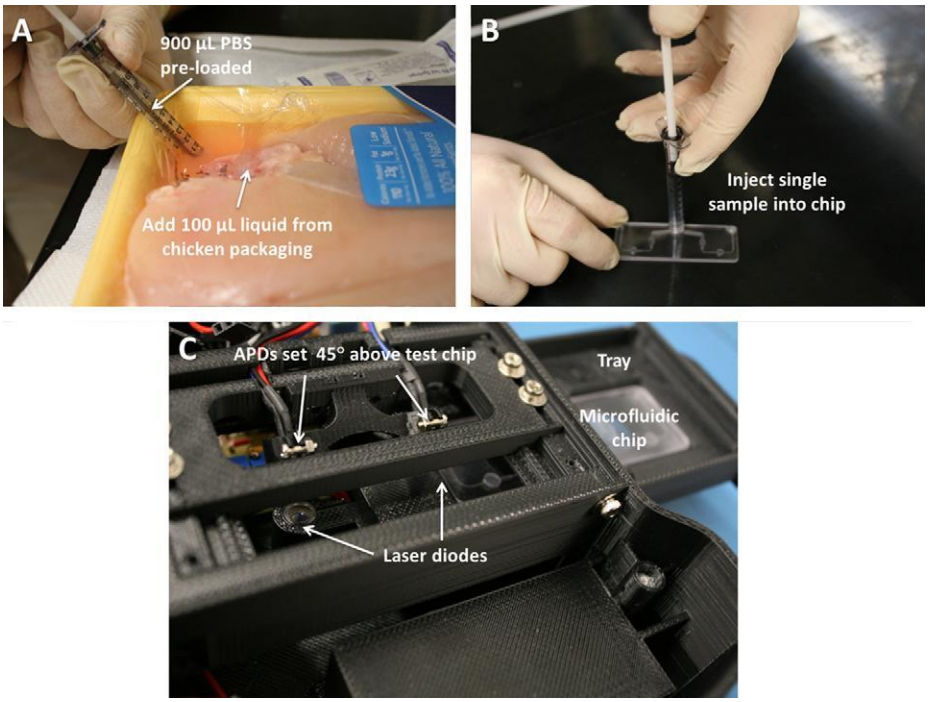

Figure 1: Overview of the assay. (A) A disposable syringe, pre-filled with 900 µL PBS, is taking 100 µL of liquid from poultry package, thus diluting it to 10%. 1% dilution is achieved in a similar manner. (B) The resulting dilution is applied directly, without any pre-processing, into the shared inlet of a microfluidic chip. (C) Detail view of a handheld device that measures Mie scatter intensities from a microfluidic chip, showing the laser diodes (650 nm) as light source, APDs and photodetector (angled at forward 451), and the retractable tray that accommodate a microfluidic

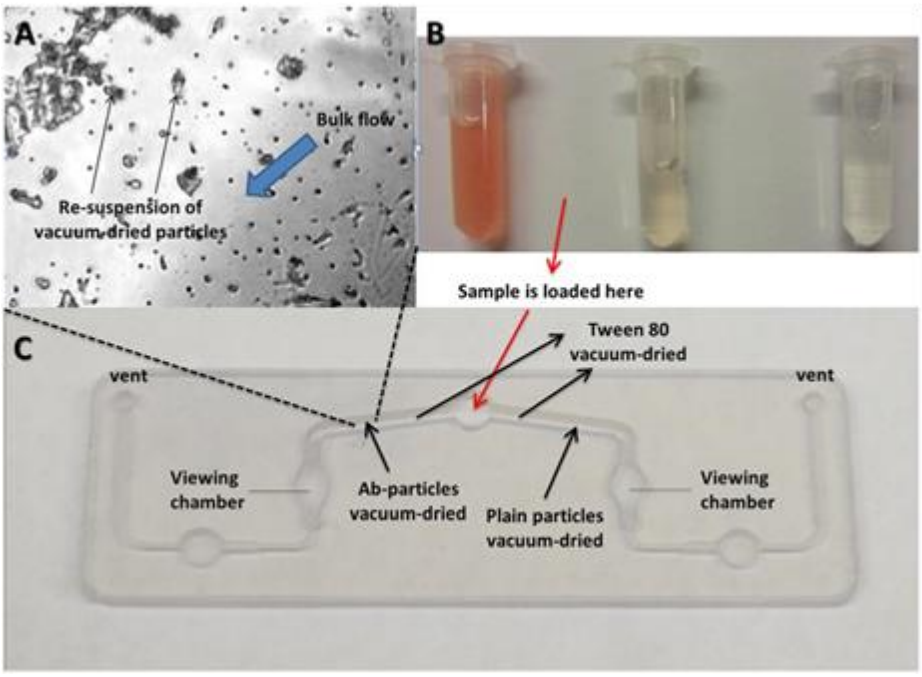

Figure 2: Microfluidic chip with vacuum-dried particles. (A) Microscopic image showing that the vacuum-dried antibody-conjugated particles are resuspending into the microchannel upon introduction of the sample. (B) Raw, 10% and 1% diluted chicken matrices. (C) The microfluidic chip. Sample is loaded into the central inlet, splitting into two channels, one with antibody-conjugated and the other with plain (unconjugated) or BSA-conjugated particles, both vacuum-dried in the channels. Tween 80 solutions are also vacuum-dried in the channels but in the different locations.

was used for the milling, and the code was generated using Surfcam 5.2 software (Surfcam, Camarillo, CA, USA). The chips contain multiple layers: the channel cutout, the bottom casing, and the top casing, which includes vents. The central layer contains HR90445 adhesive to prevent leaking. Fig. 2C shows the schematic of a microfluidic chip. For preliminary optimization purpose, a two-well chip (Fig. 3 inset) were also fabricated in the same manner, where the volume of each well was 30 mL.

920 nm mean diameter polystyrene latex microparticles (Bangs Laboratories, Inc., Fishers, IN, USA) were used as the agglutination agents in the assay. Rabbit polyclonal antibodies to the *Salmonella* Typhimurium group antigen (Abcam Inc., Cam-bridge, MA, USA) were covalently bonded to the microparticles for 100% coverage following a protocol used in a previous study (Bangs Laboratories, 2008; Heinze and Yoon, 2011). In typical immunoassays, a separate negative control is required, i.e., the same chicken matrix with no Salmonella target. Such a negative control is not only difficult to prepare but also requires refrigeration. Therefore, we used ‘‘control’’ particles and the same sample (Salmonella-spiked chicken matrix) to obtain negative control readings. These control particles were used either without any conjugation or with bovine serum albumin (BSA) conjugation with 33% coverage following the same method.

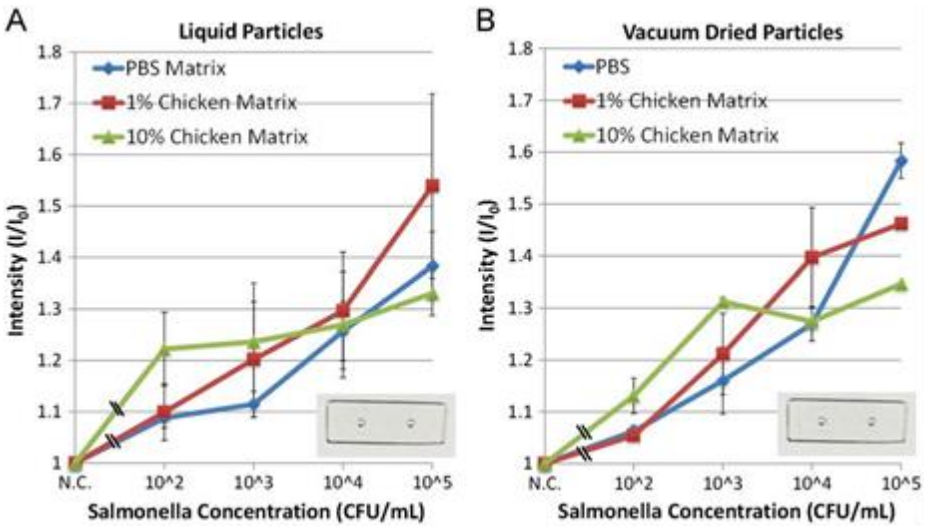

Figure 3: Liquid suspension vs. vacuum-dried particles. (A) Normalized light scatter intensities against the *Salmonella* concentrations in CFU mL^{-1} in three different sample matrices, using antibody-conjugated particles in liquid suspension in a two-well chip (shown as an inset). (B) The same with vacuum-dried particles. Averages of three different experiments.

2.5. Vacuum drying preparation of antibody-conjugated particles in microfluidic chip.

10 mL of the anti-*Salmonella* conjugated particles were loaded in the microfluidic channel along with 0.02% (for PBS and 1% chicken matrix) or 0.04% (for 10% chicken matrix) Tween 80 surfactant solutions. The locations of particle and Tween 80 loading are shown in Fig. 2C, where the target solution hit Tween 80 first, followed by antibody-conjugated particles. In addition, 10 mL 33%-BSA-conjugated particles were loaded in the micro-fluidic channel, with 0.04% Tween 80. Care was taken not to mix the particles and surfactant when loading them into the micro-channels. The loaded particles were dried overnight in a clean vacuum desiccator chamber (Ted Pella Inc., Redding, CA, USA) with a 0.02 horsepower (HP) vacuum pump (Barnant Co., Barrington, IL, USA).

2.6. Immunoagglutination assay in benchtop optical detection system.

The benchtop optical detection system was also used to optimize parameters and collect preliminary results, which was previously described in Heinze and Yoon (2011). Briefly, the microfluidic/two-well chip was situated on a flat platform using three axes, and red light emitting diode (LED) light source (650 nm) (Ocean Optics, Dunedin, FL, USA) was used to irradiate the sample. A fiber optic cable and USB4000 miniature spectrometer (Ocean Optics) were used with SpectraSuite software (Ocean Optics) to measure the light scattering intensity of the sample. For testing with vacuum dried particles, a 30 mL sample in each of the three matrices (PBS, 10% and 1% diluted chicken matrices) was introduced into the chip. The Salmonella concentrations in the spiked samples used for testing ranged from 0 (blank in PBS or negative control in chicken matrix) to 10^6 CFU mL^{-1}. For testing with liquid particles, 7 mL particles were combined with 21 mL spiked matrix liquid and 2 mL 0.02% or 0.04% Tween 80 (see Section 2.4 for the Tween 80 concentrations used).

The final concentration of particles in these mixtures was always set to 0.01% w/v. In both cases, all three matrices were used, and tests included blanks (for PBS) and negative controls (for chicken matrices). Measurements of scattered light intensity were recorded, and all readings were normalized by dividing them with blanks or negative controls. Standard curves were constructed by plotting the normalized scattered light intensity against the *Salmonella* concentration. Measurements were taken once every second for up to 6 min using SpectraSuite software and were averaged for a certain duration of time (e.g., from 3 to 6 min after target injection). Measurements were taken in triplicate, and data points were averaged together to generate standard curves. For real-time monitoring of scatter intensities, the measurements were occasionally made up to 15 min.

2.7. Particle storage stability study

The stability and shelf life of vacuum-dried, antibody-conjugated particles within the two-well chips were assessed in three conditions over a 12-week period. The conditions were tightly controlled at room temperature, refrigerated temperatures (3–8 1C) and elevated temperatures (51–55 1C) in a convection oven. Antibody-conjugated particles and 0.02% Tween 80 were loaded into the chips and vacuum dried as previously described. The loaded chips were tightly sealed and stored in their appropriate conditions. The testing matrix used was 50 mM (pH 7.4) PBS, the target Salmonella concentrations were $0–10^6$ CFU mL^{-1}, and measurements were recorded on the benchtop system after 4, 8, and 12 weeks. Stability was determined by the signal intensity loss at each temperature with increasing time.

2.8. Immunoagglutination assay in optical handheld system

The purpose of testing using this handheld device was to demonstrate that efficient field testing is possible with the system, including the microfluidic chips pre-loaded with particles, single-pipetting of sample matrix, and no sample processing. Testing was in 10% chicken matrix, including the negative control, and 0.04% Tween 80, using the vacuum dried anti-Salmonella particles and 33% BSA-conjugated particles in microfluidic channels. Measurements from both channels were taken simultaneously for the duration of 12 s, beginning 3 min after the sample was introduced. The circuitry was powered off for the initial 3 min to avoid self-heating issues of APDs. A standard curve was generated from the data.

3. Results and discussion

3.1. Benchtop detection system using two-well chip

The scattering detection angle was optimized on the benchtop device prior to each round of testing. 45° worked the best, which is analogous to our own previous works (Song et al., 2011; You et al., 2011), and used throughout the rest of this study. 650 nm light source also worked well, since the chicken matrices looked red (Fig. 2B). This red coloration comes primarily from hemoglobin and myoglobin found in chicken matrices, which absorbs blue and green but scatters/transmits red. Fig. 3A shows standard curves using liquid anti-*Salmonella* particles in the presence of the Z005 strain in the three sample matrices, using two-well chips. Again, all data points are normalized to that of a negative control (unspiked chicken matrices) or a blank (for PBS matrix). Negative controls and

blanks were measured for each set of experiments, since the chip geometry and other experimental conditions varied from experiment to experiment. Measurements were made typically less than 30 s since the readings were mostly stable over time. The curve shows good statistical difference from negative controls or blanks, with the [average – 2 × standard error] all higher than 1. Note that the negative controls and the blanks do not have error bars, since all measurements were normalized with them. The lowest concentration tested was 10 CFU mL^{-1}, a detection limit of this assay. A good signal increase was observed in all three matrices. A higher surfactant concentration was included in 10% matrix because early results suggested that non-specific interactions between the microparticles and matrix proteins overcame the immunoagglutination. The curve in 10% matrix shows a possible ‘‘dip’’ at 10^2–10^3 CFU mL^{-1} in the two-well chip, concurrent with previous studies (Heinze and Yoon, 2011), which is purely an optical phenomenon unique to Mie scattering. In Heinze and Yoon (2011), Mie scatter intensity was plotted against the particle growth parameter, where the scatter intensity increased up to 2.2 particle growth parameter, followed by a dip around 2.7 particle growth parameter, and increased again up to 3.2 particle growth parameter. Therefore, the presence of dip with 10% matrix may indicate the growth of particles to triplets or bigger, while the non-presence of dips with 1% matrix and PBS may indicate that Tween 80 was efficiently limiting the growth of particles to doublets.

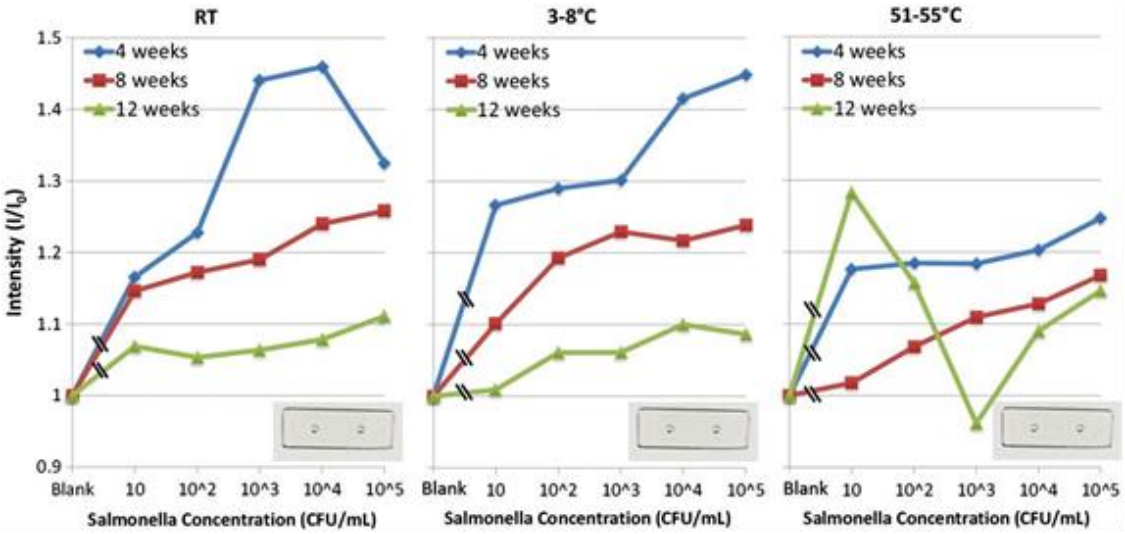

Figure 4: Long-term storage study. Normalized light scatter intensities against the Salmonella concentrations using the vacuum-dried particles, stored for 4, 8 and 12 weeks in room temperature (RT), 3–8 °C, and 51–55 °C. Two-well chips (shown as an inset) and PBS matrix were used. Averages of three different experiments. Error bars are standard errors.

Presumably, the increased surfactant concentration in the 10% matrix was not sufficiently high enough to overcome this dip. The curves show an overall increase over the target concentrations and are in general linear for the tested range of target concentrations (10^4 CFU mL^{-1}). Particle immunoagglutination appears to be initially higher at lower antigen concentrations (10^2 CFU mL^{-1}) in the presence of 10% matrix, likely due to non-specific interactions. Standard curves typically became saturated at 10^5 CFU mL^{-1}, attributed to the antigen (*S.* Typhimurium) saturation over the available antibodies on the particles.

Fig. 3B shows standard curves using the vacuum-dried anti-*Salmonella* conjugated particles in three sample matrices, again using two-well chips. Upon sample introduction

to the wells, the particles were allowed 3 min to passively reconstitute before taking measurements. This time was determined by the time necessary for the particles to diffuse in the presence of no antigen. This parallel test showed similar results to the test using liquid suspensions, with similar detection limit, signal increase, and a more pronounced dip at 10^3 CFU mL^{-1} in the 10% matrix only.

Both experiments demonstrate that the test yields a higher signal increase in 10% matrix rather than 1% matrix in the low target concentration. In addition, signal increase appears to be higher in the 1% matrix than in the PBS matrix for both cases, which was unexpected. While PBS is the ideal testing matrix in terms of results, it appears that the 1% matrix yields the most optimal results: largely linear trend with no ‘‘dip’’ and higher signal increase over the PBS matrix.

3.2. Stability of long-term particle storage

Shelf life is a very important aspect for particles used in field immunoassays due to potential storage conditions that are not ideal. Rather than refrigeration storage conditions, particles are more likely to be stored at room temperature or in a hot vehicle. To simulate field storage conditions, dried particles were sealed and stored at room temperature, 3–8 1C, and 51–55 1C and were tested after 4, 8, and 12 weeks in PBS. Results, shown in Fig. 4, show good signal increase in all storage conditions for the initial 8-week period. However, by 12 weeks, significant signal loss can be observed, and the antibodies stored in the higher temperatures appear to be completely denatured. This finding was expected due to the fact that, in general, denaturation temperature of immunoglobulin is around 60 °C (Vermeer and Norde, 2000). The results suggest that the ideal room temperature storage conditions should suffice for long-term particle storage, although caution should be taken

using particles 12 weeks old since they exhibited significant signal loss. Further study is needed to determine whether or not the particles stored in these conditions would yield sufficient results in the chicken matrices.

3.3. Benchtop detection system using microfluidic chip and real-time signal monitoring

The above experiments were also performed in a microfluidic chip, again using the same benchtop optical detection system, but this time with only vacuum-dried particles. Fig. 5A depicts the standard curves from the left side channel (anti-*Salmonella* conjugated particles) and the right side channel (unconjugated particles), using the same Salmonella-spiked 1% chicken matrix introduced to the shared injection point. Both signals are normalized to those with no-*Salmonella*-spiked 1% chicken matrices. The standard curve with anti-*Salmonella* conjugated particles shows a good signal increase over the range of target concentrations, while the one with unconjugated particles does not show such increase and is substantially smaller than 1. A series of t-tests were performed between these two curves, with all data points passing (po0.05). These measurements were made at a fixed time, usually at 3 min after sample introduction, but the results were somewhat unstable with substantially bigger standard errors. This instability is possibly due to the different nature and magnitude of interactions between the proteins in the matrix and the negatively charged terminal carboxyl groups on the particles. Fig. 2A shows such re-suspension under the bulk flow, as observed under a 10 X objective inverted light microscope.

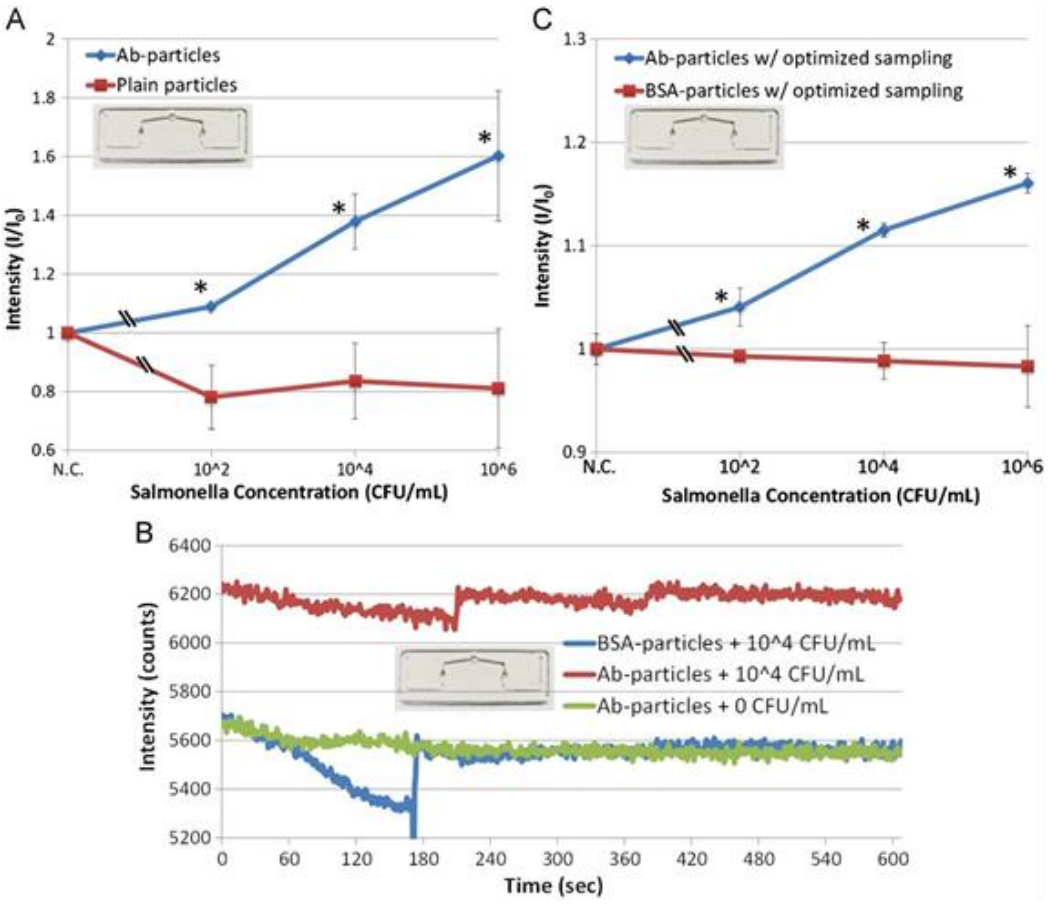

Figure 5: Plain (unconjugated) vs. BSA-conjugated particles and optimizing sampling time. (A) Normalized light scatter intensities against the *Salmonella* concentrations using the vacuum-dried particles, this time in a microfluidic chip (shown as an inset) and 1% chicken matrix. Both antibody-conjugated and plain (unconjugated) particles were used. (B) Real-time intensity changes for the select *Salmonella* concentrations and sample matrices, again using vacuum-dried particles, microfluidic chip and 1% chicken matrix. BSA-conjugated particles were used instead of plain particles. (C) Repeat of (A) but with BSA-conjugated particles and the optimized window of sampling time. Averages of three different experiments (except for B). Error bars are standard errors (except for B).

To further stabilize and particularly ‘‘passivate’’ such interactions, bovine serum albumin (BSA) was conjugated to the carboxylated polystyrene particles, instead of using unconjugated particles. BSA is (relatively) inert to immunoassays and large enough to minimize many different surface–protein interactions, and thus popularly used as a passivating protein for many different immunoassays. In addition, the ‘‘incubation time’’ at room temperature was further optimized by monitoring the real-time intensities with various samples. Fig. 5B shows select real-time intensities:

(1) 10^4 CFU mL^{-1} *Salmonella* + 33% BSA conjugated particles, (2) 10^4 CFU mL^{-1} *Salmonella* + anti-*Salmonella* conjugated particles, and (3) no target + anti-*Salmonella* conjugated particles. It is clear from this graph that more than 3 min of incubation time is often necessary depending on the sample. The target + 33% BSA conjugated particles showed roughly the same scattering intensity as did the negative control (no target + anti-*Salmonella* particles), suggesting that this protocol is suitable for calibration purposes. In addition, several different surface concentrations of BSA were tested (data not shown), with 33% being the most optimum.

Using this optimized incubation time and the 33% BSA conjugated particles, the experiments were re-performed and the results are shown in Fig. 5C. The results show desirable linear trends with the anti-*Salmonella* particles and no signal drift/ change with the 33% BSA particles, both with much smaller standard errors compared to those of Fig. 5A.

3.4. Handheld detection system using microfluidic chip

Critical to field-testing is not only ease of use, but also eliminating false positives and

negatives as well as demonstrating extremely low detection limit. From the above results, the microfluidic chip with anti-*Salmonella* and 33% BSA conjugated particles vacuum-dried in each channel, along with 0.02–0.04% Tween 80 also vacuum-dried, worked satisfactorily. An integral component to this design is a single entry well for sample input, allowing for single pipetting while minimizing assay time. In addition, this design allows for true parallel, simultaneous tests, further contributing to reproducibility.

These experiments were replicated using a handheld detection system as described in Section 2.3. This system specifically utilizes a much more sensitive light transducer, the avalanche photodiode (APD), while typical miniature spectrometers employ the linear arrays of charge-coupled device (CCD) or complementary metal oxide semiconductor (CMOS). With APDs, signals are expected to be more stable, thus maximizing sensitivity. The APDs were housed in complete darkness (within the enclosure case). To avoid self-heating and signal drift issues that are common among APDs, tests were run in reverse order, from highest to lowest target concentration (from highest to lowest voltage output).

Fig. 6A shows the results of the normalized light scattering in 10% chicken matrix. Measurements were recorded in triplicate, each from a different experiment. The data shows good linearity over the tested range of target concentration. Again, the dip at the lower concentrations was not observed, despite the fact that 10% matrix was used (there were apparent dips for 10% matrix with two well chips; see Fig. 3). Since the only difference between these experiments (Fig. 6) and those with two well chips (Fig. 3) is the use of a microfluidic chip, the unique characteristics of the newly designed microfluidic chip should be attributed to this better performance. Unlike the two well chip, there was a continuous, strict laminar flow within the microchannels, which presumably limited the

growth of particles. In addition, our unique microfluidic design allowed the sample matrix to be mixed with Tween 80 first then with the antibody-conjugated particles, while everything was mixed together in a two well chip. This sequential mixing potentially provided a surfactant-starving condition to particle immunoagglutination, thus yielding better control of particle growth. This laminar flow and sequential mixing synergistically maximized the efficiency of Tween 80 in breaking up triplet or bigger agglutinates (and possibly non-specific aggregates as well) in the sample. More research is required to determine the exact mode of immunoagglutination and non-specific aggregation.

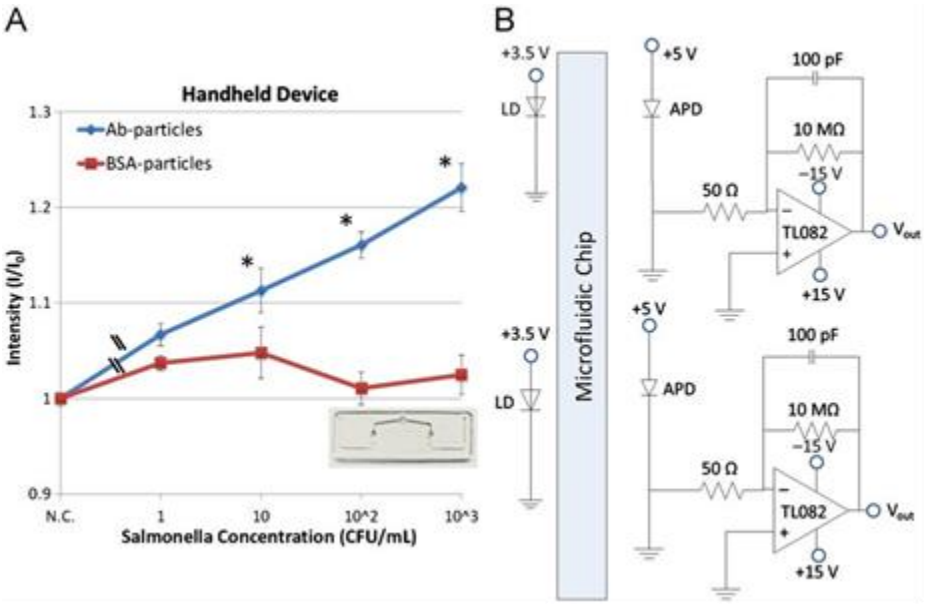

Figure 6: Assay results with final handheld device. (A) Normalized light scatter intensities (normalized output voltages in mV scale) against the *Salmonella* concentration using the vacuum-dried particles (antibody- and 33%-BSA-), microfluidic chip, 10% chicken matrix. Averages of three different experiments. Error bars are standard errors.

A series of t-tests were performed between the standard curve with anti-*Salmonella* conjugated particles and the one with 33% BSA conjugated particles. The lowest concentration with $p<0.05$ is 10 CFU mL^{-1}, indicating the detection limit of this assay. The p value for 1 CFU mL^{-1} was 0.1. This detection limit is superior or comparable to that with a comparable benchtop detection system. If a separate negative control (i.e. 10% chicken matrix with no *Salmonella* in it) can be provided, the 33% BSA conjugated particles will not be needed. In that case, the [average – 2 × standard error] for 1 CFU mL^{-1} is still higher than 1, indicating the detection limit of this assay. Note that the total sample volume was only 15 mL to each channel, indicating less than one viable *Salmonella* in each channel. This is not improbable, since anti-*Salmonella* can only bind to free antigens, cell fragments and dead cells. This extremely low detection limit was made possible through the use of APDs in conjunction with the simplified circuit design (Fig. 6B), which uses a single-stage differential op-amp with no zero adjustment. In addition, it suggests that such a device has potential use in field-testing with extreme precision. Additional modifications are required, such as circuitry to implement a normalizing algorithm, digital filtering, and liquid crystal display (LCD) panel with buttons.

4. Conclusions

This study has demonstrated a sensitive, accurate system for the detection of *S.* Typhimurium Z005 bacteria in fresh, unprocessed chicken matrices. Using Mie scattering detection, the Z005 antigen was detected in three sample matrices using two formats: the previously described benchtop device and handheld device, both in real-time. In addition, the results demonstrated that, under proper storage conditions, the conjugated particles are

viable for up to 12 weeks. We have demonstrated a system that takes advantage of single pipetting of sample into a chip pre-loaded with all necessary reagents, thus minimizing the potential of human testing error. From the operator's point of view, the whole operation involves loading the sample into a syringe that is pre-filled with PBS, unloading the diluted sample into a micro-fluidic chip, and reading the signal using a handheld device. This loading/unloading pair can be considered as single pipetting, without the need for a separate negative control, while all necessary reagents are pre-loaded into a chip. This design also allows for storage of loaded chips at room temperature. In addition, the simplified differential operational amplifier circuit, which eliminated several gain and zero-adjust stages, improved APD sensitivity, thereby minimizing signal drift. Detection limit in the various matrices for the two-well chip was 10 CFU mL^{-1}, and the detection limit in the microfluidic chip was the same using both systems. The entire assay time was approximately 10 min, including sample preparation. An advantage of this immunoassay is that detection only requires antigen rather than a whole bacterial cell, and the presence of surfactant acts to ''dilate'' the bacterial cell walls. Therefore, the Tween 80 releases extra antigen from the bacteria, increasing immunoagglutination. The presence of chicken matrix did not affect light scattering because the optical parameters (d, l and y) were optimized in order to minimize such interference. The 10% matrix required higher Tween 80 concentration due to higher interfering protein content, while the 1% matrix showed a higher signal increase over the antigen concentrations. Non-specific agglutination accounted for the slightly higher signal increase in the 1% matrix over the PBS matrix. While slight modifications are necessary, we believe that this system can be applied to point-of-care diagnostics in clinical and field settings for pathogenic testing in animal meat

samples and human whole blood, demonstrating the modularity of our system. Ultimately, this system can be applied to a wide variety of pathogens in a range of matrices, requiring only slight reagent modifications. This system has the potential to have a major impact on food processing quality control and possibly pathogen testing in humans, thereby saving the food industry millions of dollars while preventing large-scale disease outbreaks.

Acknowledgements

Funding for this work was provided by Desert Tech and the University of Arizona Office of Technology Transfer.

References

Bangs Laboratories, 2008. Techical Note #204: Adsorption to Microspheres. Bangs Laboratories, Fischers. /http://www.bangslabs.com/sites/default/files/bangs/docs/pdf/204.pdfS (accessed 13.07.2011.).

Bou, R., Grimpa, S., Guardiola, F., Barroeta, A.C., Codony, R. Poultry Science, 2006; 85: 1472–1481.

Centers for Disease Control Division of Bacterial and Mycotic Diseases, 2011. CDC Estimates of Foodborne Illnesses in the United States, Last Modified February 2 2011. /http://www.cdc.gov/foodborneburden/2011-foodborne-estimates.htmlS.

Guan, X.A., Zhang, H.J., Bi, Y.N., Zhang, L., Hao, D.L. Biomedical Microdevices, 2012; 12: 683–691.

Han, J.-H., Kim, K.-S., Yoon, J.-Y. Analytica Chimica Acta, 2007; 584: 252–259. Han, J.-H., Heinze, B.C., Yoon, J.-Y. Biosensors and Bioelectronics, 2008; 23: 1303–1306.

Heinze, B.C., Yoon, J.-Y. Colloids and Surfaces B, Biointerfaces, 2011; 85: 168–173.

Lawly, T.D., Bouley, D.M., Hoy, Y.E., Gerke, C., Relman, D.A., Monack, D.M. Infection and Immunity, 2008; 76: 403–416.

Li, A., Zhang, H., Zhang, X., Wang, Q., Tian, J., Li, Y., Li, J. Journal of Separation Science, 2010a; 33: 3437–3443.

Li, Y.Y., Zhang, C.S., Xing, D. Analytical Biochemistry, 2010b; 415: 87–96.

Lucas, L.J., Han, J.-H., Chesler, J., Yoon, J.-Y. Biosensors and Bioelectronics, 2007a; 22: 2216–2222.

Lucas, L.J., Chesler, J.N., Yoon, J.-Y. Biosensors and Bioelectronics, 2007b; 23: 675–681.

Mandal, P.K., Biswas, A.K., Choi, K., Pal, U.K.. American Journal of Food Technology,

2011; 6: 87–102.

Mairhofer, J., Roppert, K., Ertl, P. Sensors, 2009; 9: 4804–4823.

Munster, V., Wallensten, A., Olsen, B., Rimmelzwaan, G.F., Osterhaus, A.D.M.E., Fouchier, R.A.M.. In: Schrijver, R.S., Koch, G. (Eds.), In Avian Influenza: Prevention and Control. Springer, 2005; Dordrecht, pp. 25–30.

Ricciardi, C., Canavese, G., Castagna, R., Digregorio, G., Ferrante, I., Marasso, S.L., Ricci, A., Alessandria, V., Rantsiou, K., Cocolin, L.S. Food and Bioprocess Technology, 2010; 3: 956–960.

Song, J.-Y., Lee, C.-H., Choi, E.-J., Kim, K., Yoon, J.-Y. Journal of Virological Methods, 2011; 178: 31–38.

Vermeer, A.W.P., Norde, Willem. Biophysical Journal, 2011; 78: 394–404.

Zhao, J.P., Chen, J.L., Zhao, G.P., Zheng, M.Q., Jiang, R.R., Wen, J. Poultry. Science, 2009; 88: 2575–2584.

APPENDIX B

RAPID AND SENSITIVE DETECTION OF H1N1/2009 VIRUS FROM AEROSOL SAMPLES WITH A MICROFLUIDIC IMMUNOSENSOR

Hyuck-Jin Kwon,[a †] Christopher F. Fronczek,[b †] Scott V. Angus,[a] Ariana M. Nicolini,[b] Jeong-Yeol Yoon[a,b *]

a Department of Agricultural and Biosystems Engineering

b Biomedical Engineering Graduate Interdisciplinary Program, The University of Arizona, Tucson, AZ 85721-0038, USA

† These two authors contributed equally.

Published in Journal of Laboratory Automation 18 (2013) 1-10

Received 1 July 2013; received in revised form 12 September 2013; published online 2 October 2013

Abstract

Influenza A H1N1/2009 is a highly infectious, rapidly-spreading airborne disease, which needs to be monitored in near-real-time, preferably in a microfluidic format. However, such demonstration is difficult to find as H1N1 concentration in aerosol samples is extremely low, with interference from dust particles. In this work, we measured Mie scatter intensities from a microfluidic device with optical waveguide channels, where the antibody-conjugated latex beads immunoagglutinated with the target H1N1 antigens. Through careful optimizations of optical parameters, we were able to maximize the Mie scatter increase from the latex immunoagglutinations while minimize the background scatter from the dust particles. The aerosol samples were collected from a 1:10 mock classroom using a button air sampler, where a nebulizer generated aerosols, simulating human coughing. The detection limits with real aerosol samples were 1 pg/mL and 10 pg/mL, using a spectrometer or a cell phone camera as an optical detector, respectively. These are several orders of magnitudes more sensitive than the other methods. The microfluidic immunosensor readings are in concordance with the results of reverse transcription polymerase chain reaction (RT-PCR). The assay time was 30 s sampling and 5 min microfluidic assay.

1. Introduction

Influenza A H1N1/2009 is a highly infectious disease that initiated a global pandemic in 2009 (WHO, 2011). H1N1/2009 spreads through air from human respiration and/or coughing and its spread is known to be very rapid. The use of a near-real-time, field-

deployable biosensor device is the key to monitor the spread of H1N1/2009 (and other airborne viral pathogens as well). The current gold standard in detecting H1N1/2009 is reverse transcription polymerase chain reaction (RT-PCR) using the specimens collected directly from patients. Millions of copies of a specific genetic sequence from the virus can be produced with RT-PCR, ensuring low detection limit and high specificity. Specimens are typically collected from the patients' nose or throat (nasopharyngeal swab or oropharyngeal swab) (CDC, 2009). RT-PCR assay may take up to 6 hours including sample pre-processing, gene extraction, reverse transcription, thermocycling and gel imaging for product identification. This process still requires laboratory space, which adds additional time lag to sample delivery.

Field-deployable biosensors should ideally be portable, inexpensive and near-real-time. The microfluidic platform is an optimum medium to meet these requirements. In fact, a couple of works have recently been published in detecting influenza A subtype H1N1 with RT-PCR in a microfluidic format. Ferguson et al. (2011) used a specimen from a patient's throat, collected the viruses in a microfluidic channel, and ran PCR thermocycling in a small heat chamber that was connected to a microfluidic channel. Since they did not utilize the microfluidic channel for thermocycling, known as "continuous-flow PCR" (Kopp et al., 1998), their total assay time was about the same as the laboratory-based conventional PCR's: 3.5 hours. The lowest detection limit was 10 $TCID_{50}$ (50% tissue culture infectious dose), which is typical of PCR assays. Kao et al. (2011), on the other hand, did utilize the continuous-flow PCR method (but did not demonstrate the virus capture), and was able to finish the thermocycling in 75 min. Although 75 min is faster than 3.5 hours, it did not include pre-processing and product identification time, and it is

still too slow to be considered near-real-time. Their lowest detection limit was 20-30 pg/μL (= ng/mL) DNA molecules (they did not use the real virus samples). These microfluidic PCR methods do not meet the above-mentioned requirements, since they are not near-real-time and difficult to fabricate and operate.

Immunoassay-based (i.e. antibody-based) detection of H1N1 virus in a microfluidic format can provide much quicker assays, since they involve neither complicated gene extraction steps nor a lengthy thermocycling process. A couple of works have also been published recently, utilizing antibody to H1 antigens. Unfortunately, their lowest detection limits are inferior to those of microfluidic PCR methods. Lee et al. (2012) reported the detection limit of 1 μg/mL antigens using fluorescent-labeled anti-H1. Most commercial rapid kits that utilize membrane immunoassay (i.e. lateral-flow assay) show the detection limit of $10^{3.3}$ to $10^{4.7}$ $TCID_{50}$/mL (Chan et al., 2009), much inferior to the PCR methods. Li et al. (2012) used nanoparticles to improve the detection limit down to 0.5 ng/mL antigens, but they used isolated antigens rather than patient sample.

None of the above microfluidic demonstrations used specimens collected from air. In fact, studies on H1N1 virus detection from air are very difficult to find, although it is a desired method in monitoring the spread of H1N1. Coughing from the infected patient generates aerosols that contain H1N1/2009 viruses. These aerosols can be captured with a commercial aerosol sampler, but the resulting specimen contains other proteins from the patient as well as dust particles inherently found in human environments. In addition, the H1N1 concentrations in the captured aerosol samples are considerably lower than those from the patients' nose or throat.

The objectives of this research are four fold. First, a microfluidic device should be fabricated and tested for detecting H1N1/2009 viruses from aerosol samples. Second, the lowest detection limit should be as low as possible to enable the detection from such aerosol samples. Third, such detections should be made in the presence of dust particles. Fourth, the total assay time should be made as near-real-time as possible, preferably less than 10 min.

Our group has used the Mie scattering measurement of latex immunoagglutination assay, as the greater intensity change with the growth of latex beads affords lower levels of detection (Heinze et al., 2010). In a latex immunoagglutination assay, antibodies are covalently conjugated to the submicron- or micron-sized latex beads. In the presence of target antigens, antibodies are able to bridge two or more particles together, effectively "agglutinating" the latex beads, i.e. the growth of latex beads. Quantifying Mie scatter is a perfect means to monitor this growth, as it is highly dependent upon the size (and morphology) of latex beads and less dependent upon the wavelength of incident light or the concentration of latex beads. Detailed theories and equations can be found in Heinze et al. (2010) and You et al. (2011), and will be described here briefly.

When incident light hits a latex bead, it scatters light to every possible direction. The scattering angle is defined as: the same direction of incident light = forward 0° scatter; perpendicular to it = 90° scatter; back to the light source = 180° back scatter. The size of latex beads is typically submicron or micron, which is comparable to or greater than the wavelength of visible light (i.e., incident light can "see" or "recognize" an individual bead), making this particular situation fall in the Mie scatter regime. (If the bead size is sufficiently smaller than the wavelength of incident light, it becomes Rayleigh scatter.) Since the latex

bead is large enough to be recognized by the incident light, it can scatter light from multiple points, and these different scattering centers can both constructively and destructively interfere with each other. This leads to non-symmetric angular dependence of the scattered intensity for the latex beads (Kerker, 1969; van de Hulst, 1983; Bohren and Huffman, 1983). If the Mie scatter intensities are plotted against scattering angle, it will fluctuate or oscillate over the angle (which will be shown in results and discussion). Due to the different refractive indices and sizes of latex beads and the sample matrices (especially dust particles in our case), such oscillation peaks may or may not overlap with each other. We can adjust the wavelength of incident light and the size of latex beads to deliberately make such peaks not overlap with each other. This effectively enables us to maximize the scatter from latex beads and minimize the scatter from dust particles.

Performing Mie scatter detection of latex immunoagglutination in a microfluidic device provides the additional advantage of "controllability", i.e., the time-dependent immunoagglutination reaction can be precisely controlled under a strict laminar flow within a microfluidic channel.

In addition, the use of a cell phone camera as an optical detector (instead of a spectrometer) may further make the biosensor portable and easy-to-use. Cell phone cameras have recently gained popularity in chemical (Ramanathan et al., 2011) and biological sensing (Wang et al., 2011). For example, cancer cells were identified from an ELISA plate using a cell phone camera (Wang et al., 2011).

In the present study, we sought to develop a microfluidic immunosensor using a miniature spectrometer or a cell phone camera as an optical detector. Mie light scattering from immunoagglutination of antibody-conjugated, submicron latex beads was used to

quantify the amount of H1N1/2009 target in the aerosol particles captured by an air sampler. Aerosol samples were collected from a 1:10 scale mock classroom (with air conditioning/ventilation system and a nebulizer that simulates human coughing). The ability to detect H1N1/2009 virus antigens in the presence of dust particles must be demonstrated, with extremely low detection limit (substantially lower than 1 ng/mL, which has not yet demonstrated so far). This assay will be compared to the RT-PCR assay, which is the current gold standard protocol. We will do this comparison only qualitatively, since quantitative comparison between immunoagglutination assay (targeting proteins) and RT-PCR (targeting nuclei acids) would technically be incorrect.

2. Materials and method

2.1. Assay reagents and target molecules

Antibody-conjugated latex bead suspensions were used to detect H1N1/2009 from the samples in a microfluidic device. Anti-H1 (R01419, Meridian Life Science, Saco, ME, USA) was conjugated to the 920-nm highly carboxylated polystyrene beads (10.3 $Å^2$ parking area per surface carboxyl group; Bangs Laboratories, Fishers, IN, USA) by covalent binding, as described in previously research (Kwon et al., 2010). Anti-H1 specifically binds to the type 1 hemagglutinin protein on the surface of H1N1 virus capsid. We have also tested anti-N1 (type 1 neuraminidase protein), but found their binding strength (as determined by the slope of a standard curve) was inferior to that of anti-H1.

NATrol™ Influenza A H1N1 External Run Control stock (Zeptometrix Corporation, Buffalo, NY, USA; catalog number NATFLUAH1N1-ERCM), which is modified, non-

infectious virus particles from the influenza A/NY/02/2009 H1N1 strain, was used as a target.

2.2. Mie scattering simulation

Mie scattering simulations were attempted to estimate the effect of dust particles on the microfluidic immunosensor readings. Online software by Prahl (2007) was used with parameters of bead/particle diameter, refractive indices of water, latex beads and dust particles (1.33, 1.59 and 1.40, respectively), as described in previously published work (You et al., 2011). The average size of dust particles was determined by analyzing the microscope images of aerosol samples using ImageJ software (National Institutes of Health, Bethesda, MD, USA). The refractive index of 1.40 was used for the dust particles since most of the dust particles in human environment were from human skin (i.e. collagens and elastins) (Ding et al., 2006).

2.3. Fabrication of microfluidic device

The microfluidic device (with optical waveguide side-channels) used in this study was fabricated the same way as described previously (Heinze et al., 2010). The silicon master mold was single crystal silicon fabricated by photolithography and deep reactive ion etching (DRIE), where the fluidic channels were 1 mm wide and 100 μm high. To achieve a high depth pattern without any sacrificial layer, thick photoresist, AZ 4620 (~6 μm thick), was used as a silicon etching mask. During the DRIE process, C_4F_8 (110 standard cubic centimeters per minute or sccm) and SF_6 (130 sccm) with O_2 (13 sccm) were used for the passivation and etching steps. Polydimethylsiloxane (PDMS) was then poured onto the master mold and cured in a convection oven for 1 hr. The PDMS was then

peeled off the master mold, exposing the y-channel, which was subsequently bonded to a thin PDMS cover slide via oxygen plasma treatment for 2 min (Plasma Preen Cleaner/Etcher; Terra Universal, Fullerton, CA, USA). This oxygen plasma treatment causes the surface of the microchannel to become hydrophilic (water contact angle of 10° - 20°). The fluidic sample channel is a simple y-channel design, containing two inlets and one outlet, with waveguide channels in "close proximity" (separated from fluid channels by 100 μm walls). The waveguide channels were pre-filled with silicone oil (microscope immersion oil type A), where the silicone oil acts like a core (refractive index = 1.52) and the surrounding PDMS acts like a cladding (refractive index = 1.41) of an optical fiber. The critical angle of this optical waveguide is arcsin (1.41/1.52) = 68°. There is a reservoir at each inlet to load the antibody-conjugated bead suspension and the sample solution. Teflon tubing was then attached to the chip at the outlet channels to manually pump the bead suspension and sample into the y-channel by withdrawing action (at a flow rate of 10 $\mu L\ min^{-1}$).

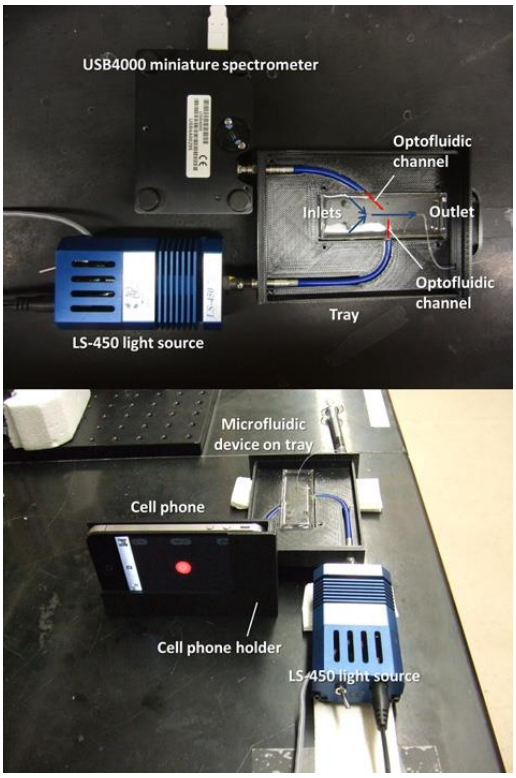

Figure 1: Microfluidic immunosensors with a miniature spectrometer (USB4000 from Ocean Optics; top) and a cell phone camera (iPhone 4 from Apple; bottom). The optical fibers were partially inserted into the optical waveguide channels, all contained within a "tray". The distal ends of optical fibers were connected to the red light-emitting diode (red LED; light source) and the detector (a miniature spectrometer or a cell phone camera) using friction fittings. Anti-H1-conjugated latex bead suspension and the diluted solution of collected air sample were separately introduced to two inlets of a y-shaped microfluidic channel, and pumped through by manually withdrawing a disposable syringe from the channel outlet. The side channels were filled with silicone oil to act as liquid core optical waveguides.

2.4. Assembly of immunosensor devices

Two types of immunosensor devices were fabricated as shown in Fig. 1, one with a miniature spectrometer (USB4000, Ocean Optics, Dunedin, FL, USA) and the other with a cell phone camera (iPhone 4, Apple Inc., Cupertino, CA, USA) as an optical detector. The disposable microfluidic device and optical fibers were placed on a "tray" as shown in Fig. 1. The tray achieved a friction fitting to the red light-emitting diode (red LED; light source) and a detector (a miniature spectrometer or a cell phone camera). Assays were performed as follows: First, the antibody-conjugated bead suspension and the sample solution were loaded to each inlet. Surfactant (Tween 80) was added to the sample solution in order to break off larger agglutinated beads, thus resulting in mostly doublets and triplets, where the scattering is maximum (see Results and Discussion) (Heinze et al., 2010; You et al., 2011). Then, these solutions were manually pumped using negative pressure created by a syringe (201000, Hamilton Company, Reno, NV, USA) that was connected to the tubing attached at the outlet. After mixing, the 640 nm red LED light (LS-450, Ocean Optics) was directed to the center of the y-channel via optical fiber and waveguide channel, which was filled with silicone oil. Forward light scattering intensity by irradiated light was collected by a detector. In cases using a spectrometer, the collected light intensity signal was sent to a laptop computer and analyzed with SpectraSuite software (Ocean Optics). In cases using a cell phone camera, images were taken every 15 s for 3 min, and each image was analyzed using ImageJ software. The image was captured at 24 bit with 5 megapixel resolution, broken into three color components of red, green and blue (RGB), each at 8 bit (0 to 255). Only the red intensities were considered. Any intensities lower than 20 were considered as background noise and neglected. All other intensities higher than 20 (out of 255) were

integrated for all 5 megapixels, and used this value as the overall red intensity (I) for a single image. These values were normalized by dividing them with the integrated red intensities from the results of PBS (I_0).

2.5. Air sampling from a mock classroom

A mock classroom was constructed with acrylic plates as shown in Fig. 2. The scale of the mock classroom is 1:10 of a real classroom at the University of Arizona. The area and volume of the real classroom is 37.96 m^2 and 94.91 m^3 respectively. Since two inlets with fans and one outlet were installed for ventilation in a real classroom, 1:10 scaled versions of inlets, fans, and an outlet were installed in a mock classroom modeled after the real ones. The fans were fabricated using the cooling fans for personal computers (35 mm × 35 mm), with the plastic enclosures designed by SolidWorks (Dassault Systemes SolidWorks Corp., Waltham, MA) and rapid prototyped with a 3D printer (Dimension uPrint SE; Stratasys Inc., Eden Prairie, MN). The flow rates from these fans were controlled by the analog voltage output from an Arduino microcontroller (Boulder, CO). The actual flow rates from the fans were measured by traceable hot wire anemometers, installed within the plastic enclosures just underneath the fans. The fans introduced the naturally occurring dust particles from the laboratory into the mock classroom. The outlet was vented into a class II biosafety cabinet with UV sterilization capability (NuAire; Plymouth, MN, USA) using 5-cm diameter plastic tubing. The upper casing of the classroom as well as the area around the base of the nebulizer was sealed for each experiment. The velocity of each fan was scaled down using the Archimedes number (Ar), as previously published (Kacira et al., 2008), using the experimentally measured velocity from the real fans. The ventilation rate of the mock classroom was 29.7 L/min or 1.05 CFM

(cubic feet per minute), which is about 7 times higher than the minimum requirement recommended by American Society of Heating, Refrigerating and Air-Conditioning Engineers (ASHRAE; 4.25 L/min = 0.15 CFM) (ASHRAE, 1997). The minimum required ventilation rate (0.15 CFM) was also applied in order to compare the signal difference caused by lower ventilation rate. No window was installed and the door was closed. A mock human was installed in order to spray aerosols that contained the modified H1N1/2009 viruses. The mock human was made of a commercial nebulizer (4650D-621, Sunrise Medical, Somerset, PA, USA), and it was installed inside the mock classroom as shown in Fig. 2. The mean diameter of aerosols that contain viruses was 5 μm according to the specification of the nebulizer manufacturer.

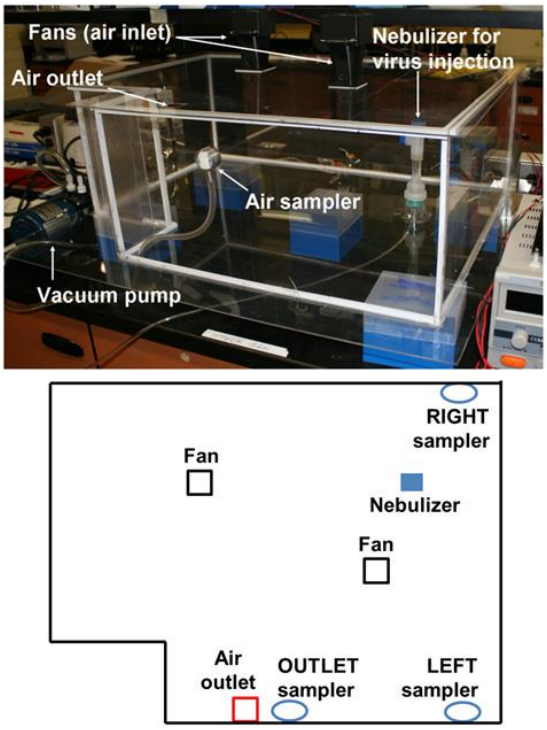

Figure 2: A photograph (top) and a top view (bottom) of a 1:10 scale mock classroom. The locations of air ventilation system (fans and outlet) and aerosol samplers ("outlet", "left" and "right") are shown.

2.6. Sample collections

The aerosolized sample injected by a nebulizer was collected with a button aerosol sampler (225-360, SKC, Eighty Four, PA, USA). The aerosol particles were injected for 3 s by pressurized nitrogen gas. The velocity of injection was 11.0 m/s. After 3 s of injection, the aerosols were transported for 3 min by the ventilation system. Then, the button aerosol sampler collected the injected aerosol samples for 30 s at three different locations (outlet, left and right; as shown in Fig. 2). This sampling time (30 s) was determined by the set of experiments that showed sufficient difference in detectable signals over three different sampling locations. The aerosol samples were captured by a filter (1820-070, Whatman, Kent, UK) inside the sampler. The filter was soaked in 150 μL of phosphate buffered saline (PBS; pH 7.4; Sigma-Aldrich, St. Louis, MO, USA) to dissolve virus particles into liquid, and then squeezed by a syringe (S7510-3, National Scientific, Rockwood, TN, USA). The button air sampler was cleaned with 70% ethanol and deionized water between each sample. A total of six sets of experiments were conducted, varying the concentrations of H1N1 virus particles inside the nebulizer (1-100 ng/mL), the ventilation conditions (29.7 and 4.25 L/min), and the three different sampling locations (outlet, left and right), each of which was replicated three times. The sampler was installed at a scaled height of 0.15 m (a typical height of human mouth, scaled down by 1:10) for all cases.

2.7. RT-PCR assays

For verification of the immunosensor readings, RT-PCR was run on aerosol samples. In the immunosensor experiments, 1-100 ng/mL solutions of H1N1/2009 virus particles were aerosolized into the mock classroom for 3 s, and the resulting concentration after sampling was 1-100 pg/mL (see Results and Discussion). Although the Mie scatter-based

microfluidic immunosensor was sufficiently sensitive to detect this low concentration, the concentration was too low to be detected with RT-PCR. Since the genome in H1N1/2009 virus particles comprised only 0.1% of the total weight, 1-100 fg/mL of the genome mass would appear in the collected aerosol samples.

Rather than increasing the concentration of virus particles for RT-PCR by 1,000-fold, which would be very dangerous and in violation of CDC regulations, genetic material was extracted from the H1N1/2009 viruses and injected into the mock classroom at high concentrations. Zymo Research Viral RNA Extraction Kit (Zymo Research, Irvine, CA, USA) was used for this extraction. Briefly, the modified viruses were denatured, and the genomic RNA was captured and purified using the filter columns provided in the kit. The final RNA elution volume was 20 µL per sample. Immediately, the RNA template was used to make cDNA using a High Capacity Reverse Transcriptase Kit (Invitrogen Life Technologies, Grand Island, NY, USA). The RT program consisted of an initial 25°C step for 10 min, a 37°C step for 2 hours, and a final 85°C step for 2 min, and random hexamer primers were used for conversion. The resulting product was 20 µL cDNA per sample and was stored at -20°C prior to mock classroom experiments.

10-50 ng/mL solutions of cDNA from H1N1/2009 virus particles were introduced into the mock classroom, under the identical conditions described in section 2.6, and this yielded approximately 10-50 pg/mL cDNA concentrations in the collected aerosol samples.

Promega 2X Green Master Mix Kit (Promega Bio-Tek, Madison, WI, USA) with DNA polymerase was used to amplify cDNA sequence. The 2009 H1N1 M gene was targeted with the following specific primer sets: MP-39-67For (5'-CCMAGGTCGAAACGTAYGTTCTCTCTATC-3') and MP-183-153Rev (5'-

TGACAGRATYGGTCTTGTCTTTAGCCAYTCCA -3') (Nakauchi et al., 2011). Up to 50 cycles were run in a conventional thermocycler (MJ Research). In order to determine PCR product, standard gel electrophoresis was performed with fluorescent imaging. Briefly, 2% agarose gel (Sigma-Aldrich, St. Louis, MO, USA) was cured and immersed in 1X tris-acetate-EDTA (TAE) buffer (Invitrogen Life Technologies), and a power supply was used to provide 120 V and 0.1 A for 45 min (Thermo Fischer Scientific; Waltham, MA, USA). Amplified samples were loaded into the gel, and 1 kbp DNA ladder (Invitrogen Life Technologies) was loaded for size comparison. The gel was soaked in ethidium bromide solution (Sigma-Aldrich) for 20 min and imaged using a Gel Doc 1000 imaging system (Bio-Rad Laboratories, Hercules, CA, USA). ImageJ software (U.S. National Institutes of Health, Bethesda, Maryland, USA) was used for image processing and band intensity determination in gray scale. Band intensity was determined by measuring pixel intensity, which was normalized to the gel background. These results were compared to those collected with the microfluidic immunosensor.

3. Results and discussion

3.1. Ability to detect the latex immunoagglutination in the presence of dust particles

A series of Mie scattering simulations was performed for both immunoagglutinated latex beads and dust particles to optimize optical parameters, namely the bead size d, the wavelength of incident light λ, and the angle θ where the scattering detection is made. Fig. 3 shows the best result, indicating that θ = 45° maximizes the scattering from immunoagglutinated latex beads while minimizing that from dust particles, for d = 920 nm

and λ = 640 nm. The size of dust particles in captured aerosol samples was measured to be on average 15 μm, evaluated from their microscope images. Mie scattering intensity of dust particles was an order magnitude lower than that of immunoagglutinated latex beads with $\theta > 40°$. Since the size of dust particles in real environment may vary, typically from 1 μm to 100 μm (WHO, 1999), it is necessary to conduct a series of simulations for varying sizes of dust particles. For the dust particles larger than 15 μm, the scattering intensity became even smaller (results not shown), hence these are not problematic. For the dust particles smaller than 15 μm (the result with 1.5 μm was shown in Fig. 3), the scattering intensity became substantially stronger for the angles smaller than 40°, while the scattering at $\theta > 40°$ remained relatively the same, with the minimum point also occurring at around 45°. This result indicates that Mie scattering light intensity of dust particles does not overlap with that of immunoagglutinated beads with the optimized scattering parameters. Therefore, it is possible to detect viral pathogens in the presence of dust particles.

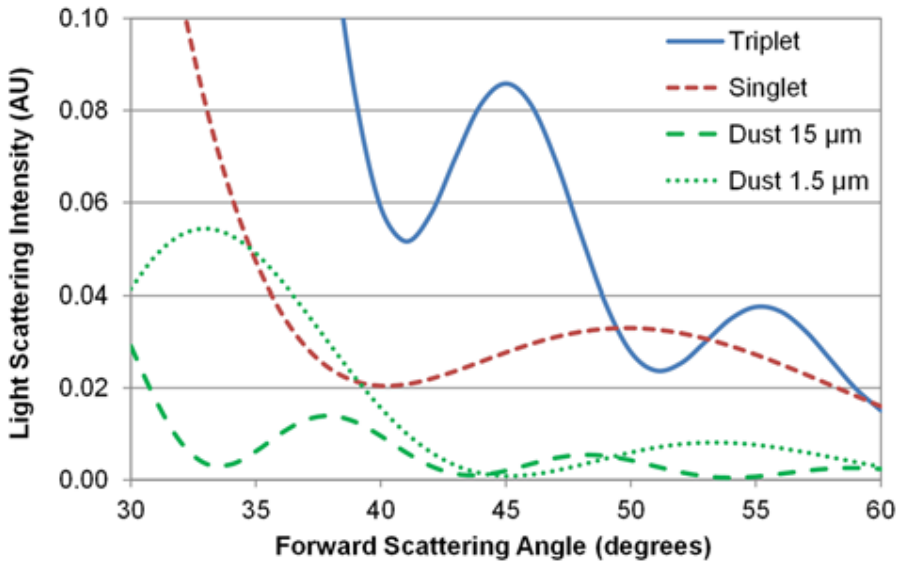

gure 3: Mie scattering simulation results for the immunoagglutinated latex beads and dust rticles. θ = 45° maximizes the scattering from immunoagglutinated latex beads while nimizing that from dust particles, for d = 920 nm and λ= 640 nm. θ < 30° was not usable due to e interference of incident light, and θ > 60° was not usable due to the reflection at the fluidic-aveguide channel interface.

3.2. Standard curves and lowest detection limits

Standard curves were constructed with serially diluted H1N1/2009 solutions in PBS (Fig. 4) using a microfluidic immunosensor with both optical detectors (spectrometer and cell phone camera). With a spectrometer, the light intensity readings (I) were recorded at 640 nm (the wavelength of incident red LED), which were divided with that of a PBS solution (I_0). The standard curve with a spectrometer detector shows a good linear trend to the logarithm of H1N1 concentration, up to 100 pg/mL, with R^2 = 0.9959. This linearity is significantly improved from the previous study (Heinze et al., 2010), through the use of optimized scattering parameters and the optimized use of surfactant (Tween 80). It seems

that Tween 80 was able to break apart larger agglutinated beads and resulted mostly in doublet- and triplet-beads, as confirmed by microscope image analysis (data not shown). The strongest scattering increase was observed with triplet agglutination as confirmed with Mie scattering simulation; if the beads are immunoagglutinated into a very big clump, the effective number of beads in the microfluidic channel is reduced dramatically, negating the effect of bead size growth. The detection limit can be determined from a standard curve by using three-sigma rule, i.e., the lower bounds of error bars multiplied by three times should be still above 1, to be statistically different from that of PBS. With this three-sigma rule, the detection limit was less than 1 pg/mL, significantly lower than most other studies (0.5 ng/mL - 1 μg/mL) (Lee et al., 2012; Chan et al., 2009; Li et al., 2012).

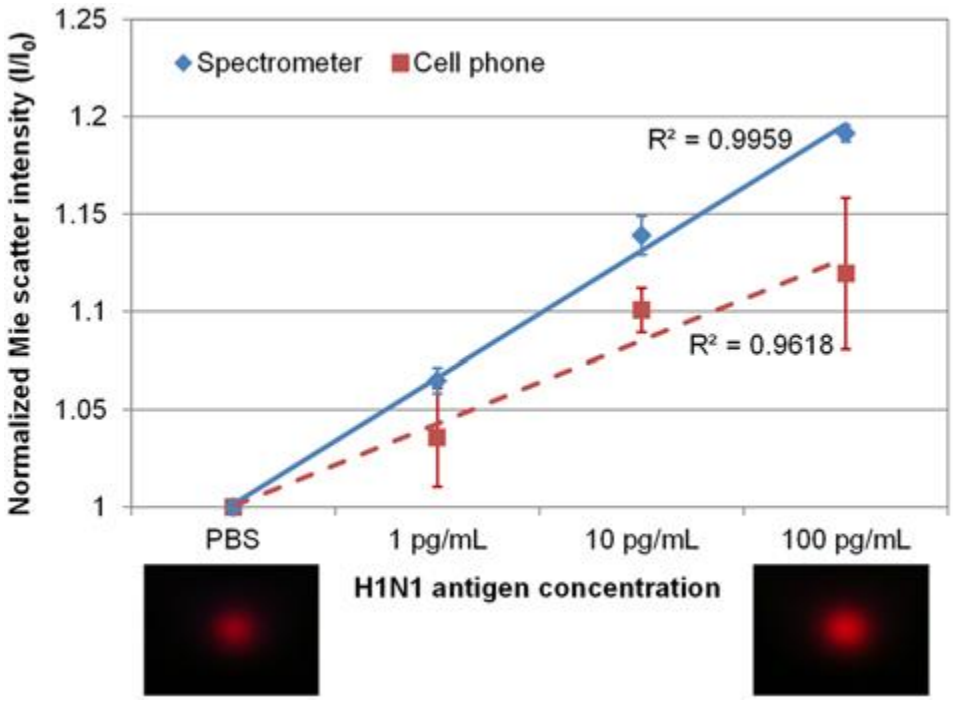

Figure 4: Standard curves constructed by microfluidic immunosensors. The detection limits were <1 pg/mL with a spectrometer and 10 pg/mL with a cell phone camera. All data points are averages of three different experiments. Error bars represent standard errors. Cell phone images from optical fibers are also shown at the bottom, for a negative control (PBS) and 100 pg/mL H1N1/2009 virus solutions, showing significant differences in brightness and area of the red spots.

The same standard curve was constructed using a cell phone camera as an optical detector. The actual cell phone images were shown underneath the graph, for PBS and 100 pg/mL H1N1 solution. It shows significant differences in brightness and area of the red spots. The red pixel intensities (above the background noise level) were integrated and used as the light intensity readings (I). These readings were again divided with that of a PBS solution (I_0). The standard curve shows a linear trend up to the logarithm of H1N1

concentration, to 100 pg/mL, but with a smaller slope, bigger error bars, and with smaller $R^2 = 0.9618$. The detection limit is 10 pg/mL, again using the same three-sigma rule. This can easily be explained with the dynamic range of analog-to-digital converters in two different systems. Despite the 24-bit image processing of a cell phone camera, it is divided amongst three different color components: red, green and blue, thus the effective resolution for red color is 8-bit (note that the system was exposed to a 640 nm red light source). The miniature spectrometer has a 16-bit resolution for all wavelengths, which is reflected in its greater sensitivity. Despite this, there is a stronger commercial potential in the cell phone camera usage as the miniature spectrometer has a price 10 times higher than that of a typical smart phone.

3.3. Immunosensor readings from collected air samples

We then detected H1N1/2009 virus antigens from the aerosol sample collected from a mock classroom. A nebulizer sprayed aerosols within a mock classroom, simulating a human coughing. The aerosols traveled through a mock classroom with the ventilation system, eventually escaped through the outlet, were trapped on the wall, or were captured by the air sampler. The button aerosol sampler collected a small portion of these aerosols at three different locations (outlet, left and right). The total amount of injected H1N1/2009 viruses was 50 pg or 5 ng, coming from 1 ng/mL or 100 ng/mL solutions in a nebulizer respectively. Two different ventilation conditions were considered, referenced to as “high” (29.7 L/min), and “minimum” (4.25 L/min), where “minimum” refers to the minimum required ventilation rate suggested by ASHRAE while “high” refers to the ventilation rate corresponding to the real classroom operation.

Fig. 5 (top) shows the normalized light scattering intensities for six different cases. For most cases, the cell phone camera detector show smaller signal compared to the spectrometer detector, consistent with the standard curves (Fig. 4). Using the standard curves (Fig. 4), all data were converted into the H1N1 concentrations, and the results are shown in Fig. 5 (bottom). After the conversion, the estimated H1N1 concentrations with a cell phone camera are not very different from those with a spectrometer, mostly within one order of magnitude difference.

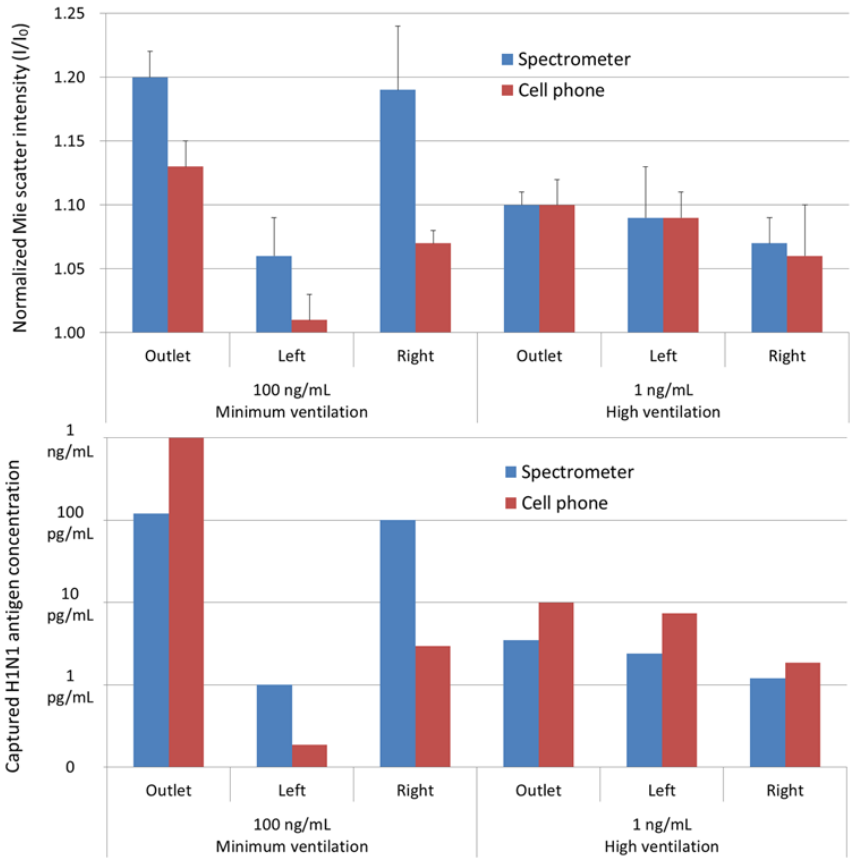

Figure 5: Top: microfluidic immunosensor readings for six different cases of experiments. All data points are averages of three different experiments. Error bars represent standard errors. Bottom: estimated H1N1 concentrations using the standard curves (Fig. 4). Both types of immunosensors show similar concentrations mostly within one order of magnitude difference.

Under the minimum ventilation condition (4.25 L/min) and high H1N1 concentration in a nebulizer (100 ng/mL), the concentrations of captured H1N1 viruses are significantly different by three sampling locations: very high at outlet and right, while very low at left. These variances can easily be explained by the unequal distribution of air by low (insufficient) ventilation condition. The H1N1 concentrations are 1-120 pg/mL with a spectrometer, or 0.19-1000 pg/mL with a cell phone camera, which are higher than those with high ventilation condition (29.7 L/min) and low H1N1 concentration in a nebulizer (1 ng/mL).

Under the high ventilation condition (29.7 L/min) and low H1N1 concentration in a nebulizer (1 ng/mL), the concentrations of captured H1N1 viruses are 1.2-3.5 pg/mL with a spectrometer, and in the order of outlet > left > right, although such differences were not very significant. In fact, these concentrations are at the detection limit of our system with a spectrometer, 1 pg/mL. The result with a cell phone camera is similar, again in the order of outlet > left > right, but with bigger variance, 1.9-10 pg/mL. This can easily be explained by the detection limit with a cell phone camera, 10 pg/mL. The total injected amount of H1N1/2009 virus was 50 pg for the 0.1 m^3 mock classroom, indicating the detection limit of our microfluidic immunosensor would be 50 pg per 0.1 m^3 volume.

Altogether, our microfluidic immunosensors are capable of correctly estimating the concentration of captured H1N1 viruses, with respect to the ventilation conditions and the H1N1 concentrations in a nebulizer. The assay time includes 30 s sampling and 5 min microfluidic assay, i.e. total of 5 min 30 s.

3.4. RT-PCR results from collected air samples

As control experiments, cDNA solutions from H1N1/2009 viruses were aerosolized into a mock classroom and analyzed using RT-PCR. From Fig. 5, we determined that the concentrations of H1N1/2009 viruses in the captured aerosol samples were 1-100 pg/mL, which was about 0.1% of the H1N1/2009 concentration in the nebulizer (1-100 ng/mL). Since the genome is only 0.1% of the total virus weight, the genomic mass in the captured aerosol samples would be only 1-100 fg/mL (= 1-100 ag/μL), which would be impossible to analyze with RT-PCR. Therefore, we used 10-50 ng/mL cDNA solutions in the nebulizer, yielding 10-50 pg/mL (= 10-50 fg/μL) cDNA in the captured aerosol samples.

Fig. 6 shows the gel electrophoresis images after 50 cycles of RT-PCR taken at three different locations (outlet, left and right), at two different ventilation conditions (high and minimum), and at various cDNA concentrations loaded in the nebulizer. Except for the cDNA concentrations, all other experimental conditions were identical to those of Fig. 5. Under minimum ventilation conditions, large amounts of cDNA were captured in the outlet and right samplers, while those captured in the left sampler were consistently smaller. Under high ventilation conditions, the amounts of cDNA captured in the samplers were as follows, from the the highest to the lowest concentrations: outlet > left > right. Both RT-PCR results (under minimum and high ventilation conditions) show the same trend found in Fig. 5 (with microfluidic immunosensors), demonstrating the capability of our microfluidic immunosensors in accurately quantifying the H1N1 viruses from the collected aerosol samples.

For both the microfluidic immunosensor and RT-PCR, the outlet sample location showed the highest amounts of targets collected. This finding is evident as the outlet

location is the nearest to the ventilation duct, so the bulk airflow movement in the mock classroom would carry a majority of the aerosols in that direction. The data also suggest that lower amounts of aerosols were collected at the left sample location, especially under minimum ventilation conditions. At the right sample location, however, there is a degree of randomness. Under minimum ventilation conditions, the immunosensor readings varied from experiment to experiment, resulting in larger error bars. They also varied due to the nature of the optical detectors (a spectrometer or a cell phone). The RT-PCR results were mixed at the right sampler location but consistently higher than at the other locations. This location is closest to the nebulizer (a mock human), despite the fact that the aerosols initially travel in the opposite direction, away from the right sampler. However, at high ventilation, collected sample concentrations were consistently lower than at the other locations, sometimes negligible, at the right location. This is due to the fact that the aerosols travel towards the outlet for the duration, while they stay in the mock classroom substantially longer than at the minimum ventilation.

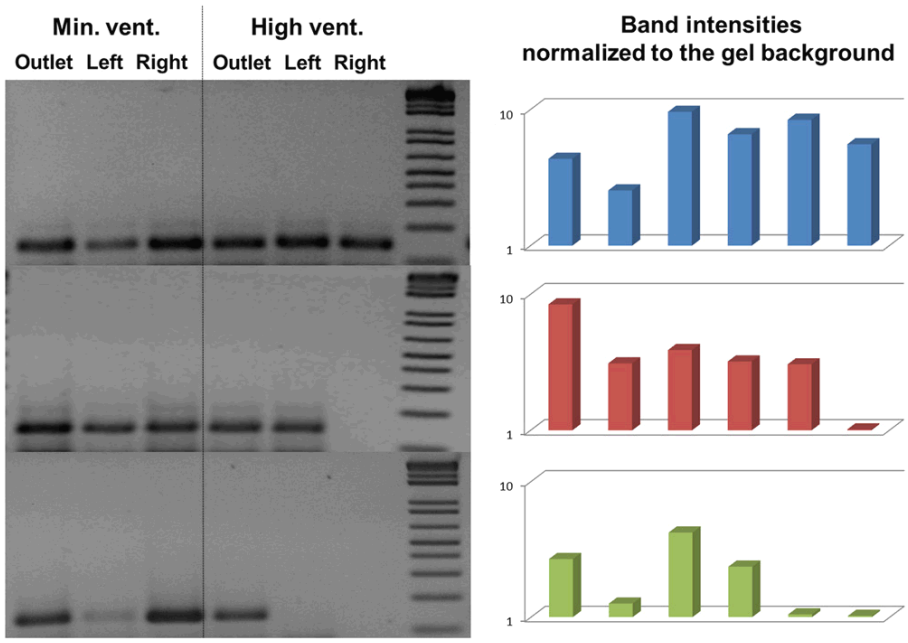

Figure 6: Gel electrophoresis images after 50 cycles of RT-PCR for the aerosol samples collected from the mock classroom, under minimum and high ventilation conditions. The cDNA concentrations inside the nebulizer were 50, 25 and 10 ng/mL (from top to bottom), and the expected cDNA concentrations in the aerosol samples were 50, 25 and 10 pg/mL = 50, 25 and 10 fg/μL. Experimental conditions are identical for each set of three gel bands. The intensities of gel bands were evaluated using ImageJ software, all normalized to the intensities of gel background.

A microfluidic device was developed to detect and quantify H1N1 viruses in the captured aerosol samples from a mock classroom. A nebulizer generated aerosols within a mock classroom, simulating human coughing. A button aerosol sampler collected aerosols at three different locations. Mie scatter intensities were measured from a microfluidic device, through optical waveguide channels, where the antibody-conjugated latex beads immunoagglutinated with the target H1N1 virus antigens. Through careful optimizations of optical parameters, we were able to maximize the Mie scatter increase from the latex immunoagglutinations while minimize the background scatter from the dust particles,

inherently found in aerosol samples. Both a miniature spectrometer and a cell phone camera were used as optical detectors, and the detection limits with real air samples were 1 pg/mL with a spectrometer and 10 pg/mL with a cell phone camera, which are several orders of magnitudes more sensitive than the other methods (which used nose or throat swab samples). The immunosensor with a cell phone camera has a higher commercial potential with a lower price tag than a miniature spectrometer. The microfluidic immunosensor readings are in good agreement with the results of RT-PCR, corresponding very well with the different ventilation conditions and the target concentrations in a nebulizer. Further work is needed to make the aerosol sampling completely automatic. A button sampler was used in this study, which is essentially a filter with a vacuum pump. A glass impinger may be used to collect aerosols into liquid, followed by automatic introduction into the microfluidic immunosensor. In addition, several different types of airborne viral pathogens need to be tested to evaluate the selectivity of the optofluidic immunosensor. The assay time includes 30 s sampling and 5 min microfluidic assay, i.e., 5 min 30 s.

Acknowledgements

The authors disclosed receipt of the following financial support for the research, authorship, and/or publication of this article: Funding for this work was provided by Animal and Plant Quarantine Agency, South Korea, award number C-AD14-2006-11-0.

References

ASHRAE (American Society of Heating, Refrigerating and Air-Conditioning Engineers). ASHRAE Handbook. ASHRAE: Atlanta, 1997.

Bohren, C. F., Huffman, D. R. Absorption and Scattering of Light by Small Particles. John Wiley & Sons: New York, 1983.

CDC (U.S. Centers for Disease Control and Prevention). Interim guidance on specimen collection, processing, and testing for patients with suspected novel influenza A (H1N1) virus infection. CDC: Atlanta. 2009. Available:http://www.cdc.gov/h1n1flu/specimencollection.htm.

Chan, K. H., Lai, S. T., Poon, L. L. M., Guan, Y., Yuen, K. Y., Peiris, J. S. M. J. Clin. Virol., 2008; 45: 205-207.

Ding, H., Lu, J. Q., Wooden, W. A., Kragel, P. J., Hu, X. H. Phys. Med. Biol., 2006; 51: 1479-1489.

Ferguson, B. S., Buchsbaum, S. F., Wu, T. T., Hsieh, K., Xiao, Y., Sun, R., Soh, H. T. J. Am. Chem. Soc., 2011; 133: 9129-9135.

Heinze, B. C., Gamboa, J. R., Kim, K., Song, J. Y., Yoon, J. Y. Anal. Bioanal. Chem., 2010; 398: 2693-2700.

Kacira, M., Sase, S., Ikeguchi, A., Ishii, M., Giacomelli, G., Sabeh, N. Acta Hort., 2008; 801: 393-401.

Kao, L. T. H., Shankar, L., Kang, T. G., Zhang, G., Tay, G. K. I., Rafei, S. R. M., Lee, C. W.H. Biosens. Bioelectron., 2011; 26: 2006-2011.

Kerker, M. The Scattering of Light and Other Electromagnetic Radiation. Academic: New York, 1969.

Kopp, M. U., de Mello, A. J., Manz, A. Science, 1998; 280: 1046-1048.

Kwon, H. J., Dean, Z. S., Angus, S. V., Yoon, J. Y. JALA, 2010; 15: 216-223.

Lee, K. G., Lee, T. J., Jeong, S. W., Choi, H. W., Heo, N. S., Park, J. Y., Park, T. J., Lee, S. J. Sensors, 2012; 12: 10810-10819.

Li, Y., Kang, Q. S., Sun, G. P., Su, L. J., Zheng, Z. H., Zhang, Z. F., Wang, H. Z., He, J. K., Huang, W. H. Anal. Bioanal. Chem., 2012; 403: 2449-2457.

Nakauchi, M., Yasui, Y., Miyoshi, T., Minagawa, H., Tanaka, T., Tashiro, M., Kageyama, T. J. Virol. Meth., 2011; 171: 156-162.

Ramanathan, N., Lukac, M., Ahmed, T., Kar, A., Praveen, P. S., Honles, T., Leong, I., Rehman, I. H., Schauer, J. J., Ramanathan, V. Atmos. Environ., 2011; 45: 4481-4487.

Van de Hulst, H. C. Light Scattering by Small Particles. John Wiley & Sons: New York, 1983.

Wang, S. Q., Zhao, X., Khimji, I., Akbas, R., Qui, W., Edwards, D., Cramer, D. W., Ye, B., Demirci, U. Lab Chip, 2011; 11: 3411-3418.

WHO (World Health Organization). Hazard Prevention and Control in the Work Environment: Airborne Dust (WHO/SDE/OEH/99.14). WHO: Geneva, 2011; pp. 1-15.

WHO (World Health Organization). Pandamic Influenza A. WHO: Geneva, 2011.

You, D. J., Geshell, K. J., Yoon, J. Y. Biosens. Bioelectron., 2011; 28: 399-406.

APPENDIX C

PAPER MICROLFUIDIC EXTRACTION OF PATHOGENIC NUCLEIC ACID FROM FIELD AND CLINICAL SAMPLES TOWARDS A DIRECT MICROTAS APPARATUS

Christopher F. Fronczek[a], Tu San Park[b], Dustin K. Harshman[a], Ariana M. Nicolini[a], and Jeong-Yeol Yoon[a,b*]

[a] Biomedical Engineering Graduate Interdisciplinary Program

[b] Department of Agricultural and Biosystems Engineering

The University of Arizona, Tucson, AZ 85721-0038, USA

Submitted to Lab on a Chip, 5 December, 2013

Abstract

A rapid, paper microfluidic-based protocol for extracting nucleic acid from *Salmonella* Typhimurium was developed for field and clinical samples, utilizing a multi-faceted paper channel. Initially, liquid samples (10% diluted) from fresh poultry packaging liquid were loaded on the paper strips and were lysed with tris-EDTA (TE) buffer. Nucleic acids from the lysed samples were eluted through the paper channel with TE buffer and three sections of paper at specified lengths were excised for the further polymerase chain reaction (PCR) assay. The extraction efficiency was determined by measuring fluorescence reflectance with either a benchtop optical detection system (consisting of an LED light source, a pair of optical fibers, and a miniature spectrophotometer, all built on micro-positioning stages) or a smartphone-based miniscope (in-house fabricated). The limit of detection of *Salmonella* Typhimuirum in 10% poultry packaging liquid extracted in cellulose paper was 10^3 CFU/mL, while that extracted in nitrocellulose paper was10^4 CFU/mL (as determined by both PCR and fluorescence reflectance). We observed that DNA migrates through nitrocellulose at a faster rate and further than through cellulose due to charge-charge repulsion between nitrocellulose and DNA (both negatively charged). We tested *Salmonella* extraction efficiency in 10% poultry packaging liquid, 10% whole blood, and 10% fecal samples, and obtained comparable extraction efficiency. Direct detection results were verified using PCR. This protocol is suitable for the direct detection of total bacteria count in a dirty sample (when specificity is not necessary) as well as determining extraction efficiency. This protocol is compatible with PCR, to provide specific information about the type of pathogen present in sample.

Keywords: Nucleic acid extraction, paper microfluidics, direct detection, fluorescence, smartphone, Salmonella, cellulose, nitrocellulose, poultry packaging liquid

Introduction

In this modern age, there has been a paradigm shift from reactive medicine to proactive medicine, and this general model includes the focus of on-site, rapid diagnostics. However, despite the advancements in field-deployable pathogen detection and point-of-care diagnostics, there is still an unacceptable level of outbreaks of common pathogens even in developed countries, originating from contaminated food, water, and air. These pathogens are often well-studied and can be very easily avoided if proper care is taken, and proper diagnostic tools would aid in the prevention of these illnesses. Many common bacterial infections, often originating from improper handling of food, lead to a large percent of hospitalizations and sometimes lead to death. These diseases cost the food and medical industry hundreds of millions of dollars per year. According to the U.S. Centers for Disease Control and Prevention (CDC), *Salmonella* species, among them *Salmonella* Typhimurium, affect nearly 50 million Americans each year and lead to the highest number of hospitalizations [CDC, 2013]. Clearly, more emphasis on on-site pathogen detection is necessary. In the past several years, much research has focused on developing on-site portable assays that maximize specificity and sensitivity while minimizing operation complexity. While the introduction of enzyme-linked immunosorbent assay (ELISA) made great strides in sensitivity and specificity, it requires several washing steps and is not user-friendly [Mairhofer et al. 2009]. Today, the gold standard for the detection of a specific pathogen is to identify its specific nucleic acid sequence. However, since clinically

relevant samples often contain very small amounts of DNA from pathogens, sequence amplification using polymerase chain reaction (PCR) is necessary [Huang et al. 2006]. PCR is generally preferable over typical immunoassays due to better sensitivity and specificity. Unfortunately, PCR is quite labor intensive and requires samples preparation, nucleic acid extraction and purification, amplification, and product identification (typically through gel electrophoresis); the whole process takes 4-6 hours. In order to lower the total assay time, various miniature devices have been established such as PCR-in-a-chip [Kopp et al. 1998; Lien et al. 2007; Takenaka et al. 2000; de Lumley-Woodyear et al. 1996; Lee et al. 2006] and microdroplet manipulation [You et al. 2011; Harshman et al., 2014]. Also, cell culture has been introduced into PCR in order to increase the concentration of nucleic acid, decreasing the number of cycles needed for PCR [Jonas et al. 2002]. However, these protocols only focus on amplification and do not account for laborious samples preparation, extraction, and detection. Generally, both ELISA and PCR require several hours of bench work, use expensive equipment, and are still laborious. Therefore, a more rapid, simple, and user-friendly apparatus that allows for sensitive and on-site pathogen detection should be developed. Because of its specificity and abundance, nucleic acid should be targeted, and a simple extraction device could provide fast sample preparation for PCR while providing a platform for preliminary detection. Direct DNA detection in microfluidic formats has been attempted, particularly in lateral flow assay format [Mao et al. 2009; Lo et al. 2013] but these techniques require sample pre-treatment, may not be compatible with real samples, often target ribosomal RNA (rRNA) but not genomic DNA, and rely on colorimetric detection. Because of these limitations, the assay requires heat in order to unfold the nucleic acid. Clearly, there is a need to directly target nucleic acid with a

simplified protocol. Paper microfluidics, an emerging field, has the potential to provide a cheap, user-friendly format for on-site detection of various pathogens in complex samples. Paper microfluidic techniques have been utilized to detect glucose [Carrilho et al. 2009], proteins [Martinez et al. 2008], and as an ELISA platform [Cheng et al. 2010]. In a recent study, a particle immunoassay for *Salmonella* detection was achieved on cellulose paper using a smart phone, and a 10 CFU/mL detection limit was achieved [Park et al. 2013]. Smart phones have been interfaced with a variety of biosensors for the optical detection of various hormones [You et al. 2013], parasites [Mudanyali et al. 2012], and bacteria [Zhu et al. 2012]. In this study, we develop an easy-to-use paper microfluidic chip to extract and isolate genomic nucleic acid (DNA) from *Salmonella* Typhimurium in real field samples (which may be used in conjunction with portable or on-chip PCR) and propose a one-step direct detection apparatus (no PCR) using a smartphone.

Materials and methods

Salmonella Typhimurium

The *Salmonella* Typhimurium Z005 strain (ZeptoMetrix, Buffalo, NY, USA) was cultured in 25 mg mL^{-1} brain heart infusion broth (Remel, Lenexa, KS, USA). It was incubated for 12 hours at 37°C with the final concentration of 8.6×10^8 CFU mL^{-1}. This bacterial culture (assumed 10^9 CFU mL^{-1}) was used to make serial dilutions in deionized (DI) water. The bacteria was re-cultured daily.

Poultry packaging liquid

Fresh chicken breasts and thighs were purchased from local stores and the fresh liquid was extracted from the packaging with no further processing. The extracted liquid samples were confirmed to be negative for *Salmonella* Typhimurium K005 using standard cell plating techniques and PCR (details discussed later). The raw samples were then used to make 10% dilutions in DI water. Poultry packaging liquid samples were stored in refrigeration and used for up to 4 weeks. For testing, the sample matrices were spiked with the serially diluted *Salmonella* Typhimurium to 10%, ensuring that the sample matrix was not further diluted. The spiked samples were placed in 2 mL centrifuge tubes at room temperature during testing.

Whole blood

Whole human blood, Type O, with heparin sulfate, was purchased from the Interstate Blood Bank (Interstate Blood Bank Inc., Memphis, TN, USA). Blood aliquots were diluted to 10% in DI water. Samples were stored in refrigeration for up to four weeks. For testing, the samples were spiked with 10^5 CFU/mL serially diluted *Salmonella*.

Fecal matter

Fecal samples from an African Spurred tortoise, swabbed from the floor of a habitat, were collected and placed in a centrifuge tube containing DI water. Further dilutions were necessary to achieve 10% dilution. Fecal samples were tested for the presence of *S.* Typhimurium for negative confirmation. Samples were stored in refrigeration for up to four weeks. For testing, the samples were spiked with 10^5 CFU/mL serially diluted *Salmonella* Typhimurium.

Fabrication of paper microfluidic chips

Microfluidic channels were patterned on paper using a standard lithography technique with UV development [Martinez et al. 2008]. Channels were designed using SolidWorks 2010 (SolidWorks Corp., Concord, MA, USA) and were printed on clear transparency film to form a mask. Whatman cellulose #1 and nitrocellulose paper (Whatman Ltd., Kent, UK) strips were immersed in thinned SU-8 2075 negative photoresist and were UV-exposed with the mask following pre-baking. The paper chip was rinsed with acetone and isopropyl alcohol (Sigma Aldrich, St. Louis, MO, USA), and the resulting hydrophilic channel consisted of a square loading site (7 mm × 7 mm), a channel for filtration (4 mm × 30 mm) and an absorbent pad (Fig. 1). All chips were kept in a sterile environment and free of dust particles.

Sample loading onto paper microfluidic chips

Aliquots of cultured *Salmonella* Typhimurium (some spiked in 10% poultry packaging liquid) were loaded on the inlets of paper strips (Fig. 1a), and Tris-EDTA (TE) buffer (pH 8.0; Sigma-Aldrich) was loaded for lysis (Fig. 1b). Samples were allowed to incubate for three minutes, followed by an elution in TE buffer (Fig. 1c). At this point, the eluted sample was either loaded for conventional PCR, or the entire chip was analyzed using fluorescent reflectance detection.

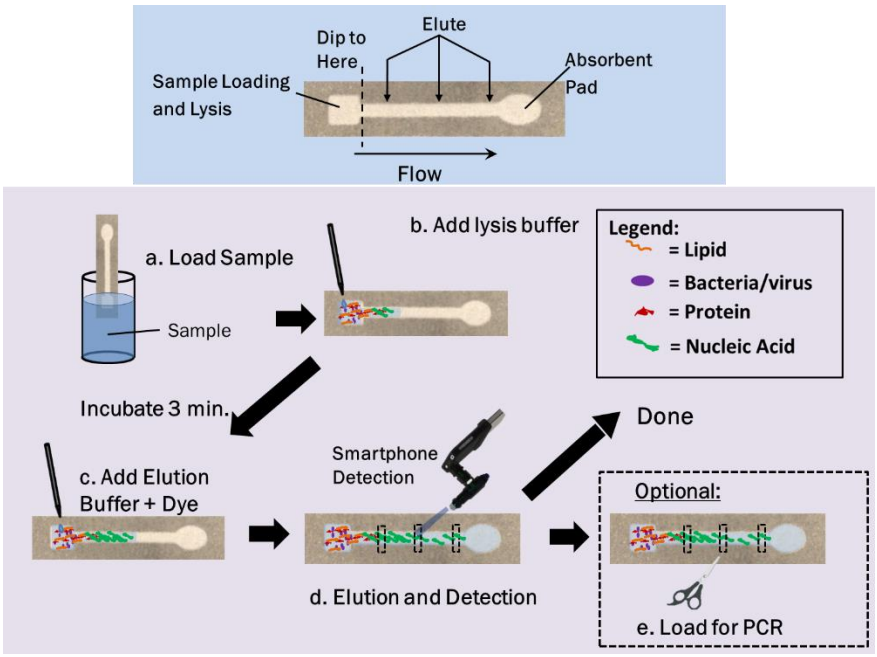

Figure 1. Patterned cellulose channel using modified lithography with equally-spaced elution regions. The overall sample preparation is as follows: (a) load sample on paper; (b) add TE lysis buffer and incubate for 3 minutes; (c) add TE elution buffer and intercalating dye; (d) elute nucleic acid and measure fluorescence reflectance signal with smart phone; OPTIONAL: (e) excise specific paper regions and load nucleic acid in pre-mixed solution of PCR reaction. The flow shows theoretical separation of various components within paper.

Direct fluorescence detection with benchtop system

For direct detection, the chip containing eluted nucleic acid was fastened to a plastic reader device (Fig. 3a), fabricated using a Dimension uPrint 3-D printer (Stratasys, Inc., Eden Prairie, MN, USA). 2 µL of Qubit dye (very sensitive, fluorescent intercalating dye; Invitrogen Life Technologies, Carlsbad, CA, USA) was loaded at 3 pre-determined locations along the paper channel. The dye loading and chip imaging were performed in the dark using a benchtop positioning stage with a 475 nm LED light source (LS-450;

Ocean Optics, Dunedin, FL, USA) and a miniature spectrophotometer (USB4000; Ocean Optics) (Fig. 3a). Fiber optic cables (Ocean Optics) were used to guide the blue excitation light from the LED light source perpendicular to the chip regions of interest, and the green emission light to the miniature spectrophotometer (USB4000), collected at a pre-determined 85° angle from the chip, or 5° from the excitation (Fig. 3a). This angle was determined to minimize the direct reflectance from the paper while receiving maximum fluorescent emission from it. *Salmonella* in clean culture broth and in 10% poultry packaging liquid were loaded onto cellulose and nitrocellulose strips, and lysis and elution were carried out using TE buffer. Without allowing the strips to dry, Qubit dye (this is an intercalating dye that binds to double stranded DNA and subsequently fluoresce, just like SYBR Green but much more sensitive) was loaded onto the three testing regions, and direct fluorescence detection was performed on the aforementioned benchtop reader system. To switch between detection zones, the holder was moved horizontally along a track so that the incident and detection angles remained constant. Signals were normalized to a negative control consisting of DI water and dye, and standard curves were constructed from the data.

Direct fluorescence detection with smartphone

Fluorescent signals were detected on patterned cellulose chips using an iPhone 4 (Apple Inc., Cupertino, CA, USA) and a fluorescent miniature microscope attachment fabricated in our laboratory, hereafter termed "miniscope," (Fig. 7). The scope contains two 10X objective lenses for focus (CAT. No. LA1560-A) (Thor Labs, Newton, NJ, USA), 492 nm bandpass filter (CAT. No. 65-087) (Edmund Optics Inc., Barrington, NJ, USA), 520 nm bandpass filter (CAT. No. 65-093) (Edmund Optics), and 500 nm dichroic shortpass filter (CAT. No. 69-178) (Edmund Optics). A blue LED was used to create

lighting, and the CMOS camera of a smartphone captured the high resolution images. Briefly, three concentrations of *Salmonella* were spiked into 10% poultry packaging liquid, and lysis and elution were performed in cellulose and nitrocellulose strips. Qubit intercalating dye was added to the optimal zone 2 region on the chip. Images were taken with the iPhone and the aforementioned miniscope. ImageJ software was used to determine the green pixel intensity, and these values were used to form a standard curve normalized to the negative control (the 10% poultry packaging liquid without *Salmonella*). Experiments were replicated in triplicate. In addition, 10% whole blood and 10% fecal samples were tested in addition to the 10% poultry packaging liquid. These additional samples were spiked with 10^5 CFU/mL *Salmonella*, and points were normalized to a negative control for each sample. Again, testing in both cellulose and nitrocellulose was in triplicate.

Conventional PCR for verification

Target nucleic acid was eluted from the paper channels by excising specific portions of the channel, followed by dipping in and rinsing with TE buffer. The resulting bacterial genomic DNA was amplified with conventional PCR, using 2X Promega Green Master Mix (Promega Corporation, Seattle, WA, USA), for 35 cycles on a conventional thermocycler (MJ Research, Walthman, MA, USA). The following primer sets were used to target the Z005 genome: sal201F (5'-CGGGCCTCTTGCCATCAGGTG-3') and sal597R (5'-CACATCCGACTTGACAGACCG-3'). Standard gel electrophoresis with ethidium bromide fluorescent staining was used for amplicon determination. Cured 2% agarose gel (Sigma-Aldrich) was immersed in 1X tris-acetate-EDTA (TAE) buffer (Invitrogen Life Technologies), and a power supply provided 120 V and 0.1 A for 45 min

for electrophoresis (Thermo Fischer Scientific; Waltham, MA, USA). Amplified samples were loaded into the gel along with 1 kbp DNA ladder (Invitrogen Life Technologies). The gel was soaked in ethidium bromide solution (Sigma-Aldrich) for 20 min and imaged using a Gel Doc 1000 imaging system (Bio-Rad Laboratories, Hercules, CA, USA). ImageJ software (U.S. National Institutes of Health, Bethesda, Maryland, USA) was used for image processing.

Results and discussion

Salmonella extraction from poultry packaging liquid

Conventional PCR was used to verify that DNA was successfully extracted from *Salmonella* on cellulose and nitrocellulose paper channels. Negative controls were 10% poultry packaging liquid, free of bacteria, loaded onto the chip. An elution step was performed at the three regions of interest on the paper, and gel results for *Salmonella* at various concentrations in 10% poultry packaging (Fig. 2) are shown at the expected 400 bp product length. The gels suggest a 10^3 CFU/mL detection limit in cellulose paper (Fig 3a), well below the infectious dose [Lawly et al. 2008], and lower than the 10^4 CFU/mL detection limit in nitrocellulose paper (Fig. 2c). This difference in detection limit is due to the superior filtration properties of cellulose paper. In addition, motility of DNA through both paper types was observed. Gel results suggest that DNA migrates through nitrocellulose farther and faster than through cellulose channels. This is likely due to the fact that the *Salmonella* Typhimurium genome is quite large (4.87 Mbp), and nucleic acid may be physically entrapped within cellulose fibers. However, nucleic acid will not

preferentially interact with nitrocellulose but will instead be repelled through charge-charge repulsion (both nitrocellulose and DNA are negatively charged) [Munster et al. 2005]. For this reason, target DNA will travel through nitrocellulose further than through cellulose. The data preliminarily suggests that a majority of DNA is captured at zone 2 in cellulose and zone 3 (furthest section in channel from loading site) in nitrocellulose. Both types of paper are suitable for extraction and direct detection due to their wettability.

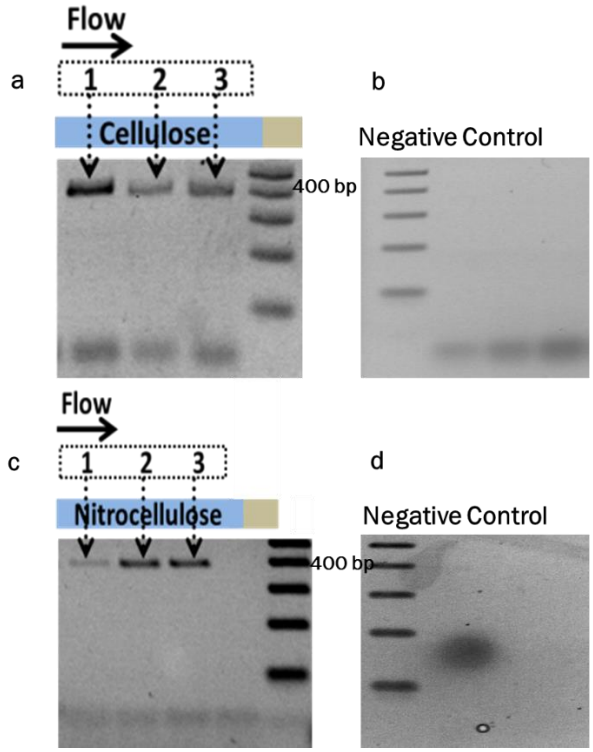

Figure 2: PCR verification gels. Cellulose (a) and nitrocellulose (c) paper extraction, of Salmonella (103 CFU/mL) and (104 CFU/mL), respectively, spiked in 10% poultry packaging, eluted at three regions along the paper channel. Bands occurred at the expected 400 bp product length. Negative controls for (b) cellulose and (d) nitrocellulose extraction, with unspiked 10% poultry packaging liquid loaded. This set of experiments illustrates the movement of large target DNA (4.86 Mbp) was faster through nitrocellulose compared to cellulose. Limit of detection is 103 CFU/mL through cellulose and 104 CFU/mL through nitrocellulose.

Direct fluorescence detection

Towards creating a field-deployable diagnostic tool to 1) collect preliminary data on total bacteria count in a sample or 2) check for successful DNA extraction from a sample, fluorescence reflectance measurements were made using Qubit intercalating dye and a benchtop spectrophotometer system (Fig. 3a). In order to minimize interfering backscatter signal caused by the wet paper, the detection angle was set to 85° from the paper (5° from the incident light) in order to minimize backscatter from the paper. Green fluorescence reflectance was measured using Qubit intercalating dye to determine DNA extraction efficiency from clean *Salmonella* culture (in DI water) using cellulose (Fig. 3b) and nitrocellulose paper (Fig. 3c), over three different locations of a paper channel.

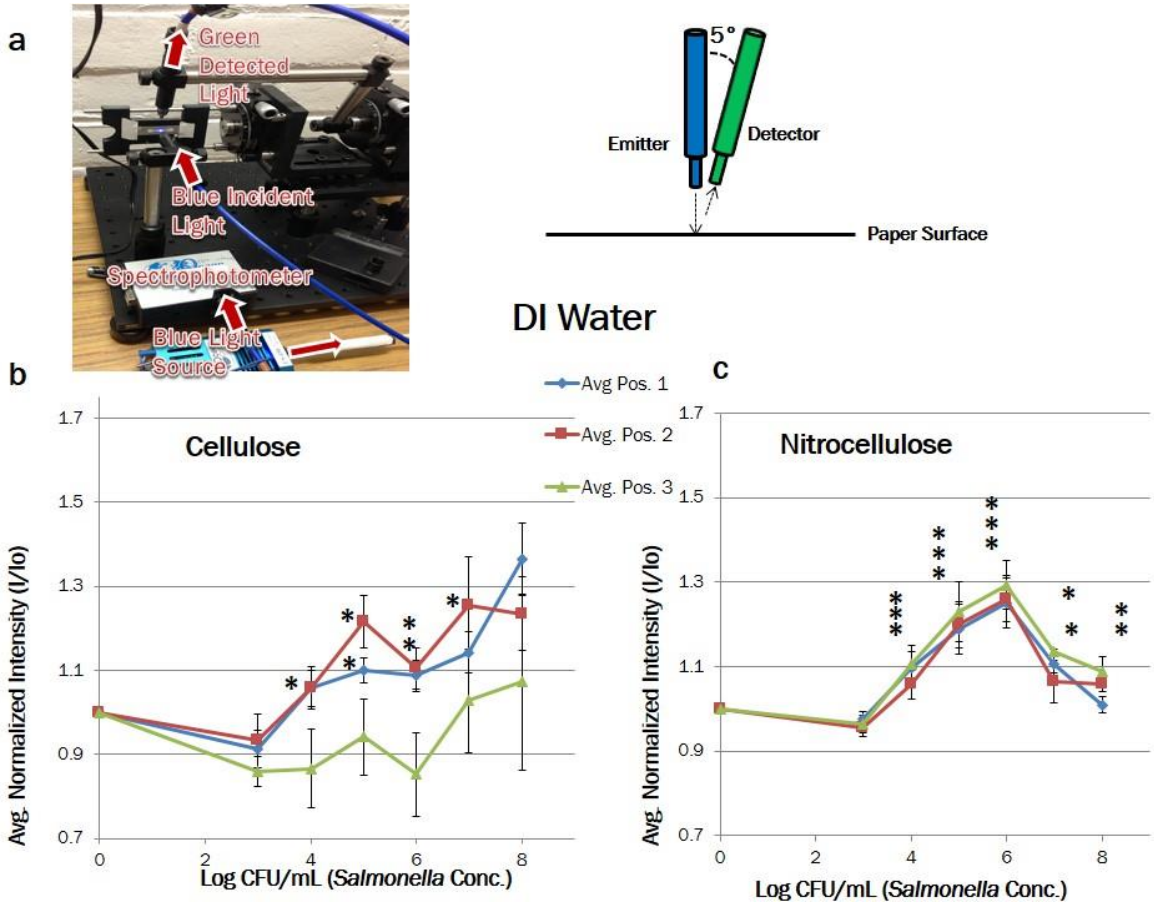

Figure 3: Fluorescent reflectance intensities taken on positioning stage **(a)**, using intercalating dye, from clean *Salmonella* (in DI water) DNA extraction on **(b)** cellulose and **(c)** nitrocellulose paper chips. Samples were normalized to a DI negative control to create a standard curve (n = 3). The DNA can move farther on nitrocellulose paper than through cellulose paper due to charge-charge repulsion between the negatively charged nitrocellulose and negatively charged DNA backbone. Clogging occurs in cellulose paper due to bacterial colony formation and some unlysed cells, creating a dip at 10^6 CFU/mL. This dip occurs at a higher concentration on nitrocellulose paper because of the lack of filtration.

Similarly, DNA extraction efficiency was determined from *Salmonella* spiked in 10% poultry packaging liquid in cellulose (Fig. 4a) and nitrocellulose paper (Fig. 4b). Total assay time was five minutes. Standard curves, normalized to DI water and the negative control of poultry packaging liquid, showed a good increase in scattering intensity with increasing pathogen concentration. Negative controls were taken for each set of experiments due to the variation in paper chips as well as experimental conditions. Cellulose extraction of clean *Salmonella* and *Salmonella* spiked in 10% poultry packaging liquid yield a detection limit of 10^3 CFU/mL, which is in good agreement with the PCR gel results (Fig. 2). These curves also show the average maximum signal intensity output over the range at zone 2, which is also in concordance with the PCR gel data (Fig. 3). However, there is a dip in signal for zones 1 and 2 around 10^6 CFU/mL, which can be explained by *Salmonella* colonizing and therefore clogging the paper fibers. This colonization was consistently observed under a light microscope with 40X objective lens. The normalized fluorescent intensity starts to re-increase beyond 10^7 CFU/mL, presumably because there are enough available cells present to yield enough DNA to bypass the clogging. This

clogging may become a larger obstacle when using poultry packaging liquid due to the interfering components of the sample. However, the results shown in Fig. 4a show similar trend, with even less apparent dips. Possible explanations include: 1) the standard curve was normalized to negative control comprised of the poultry packaging liquid free of bacteria, and 2) proteins from poultry packing liquid, especially albumin and phospholipids (debris of lysed cells), acted as stabilizing agents or natural surfactants that reduced additional clogging, thereby achieving sufficient extraction efficiency.

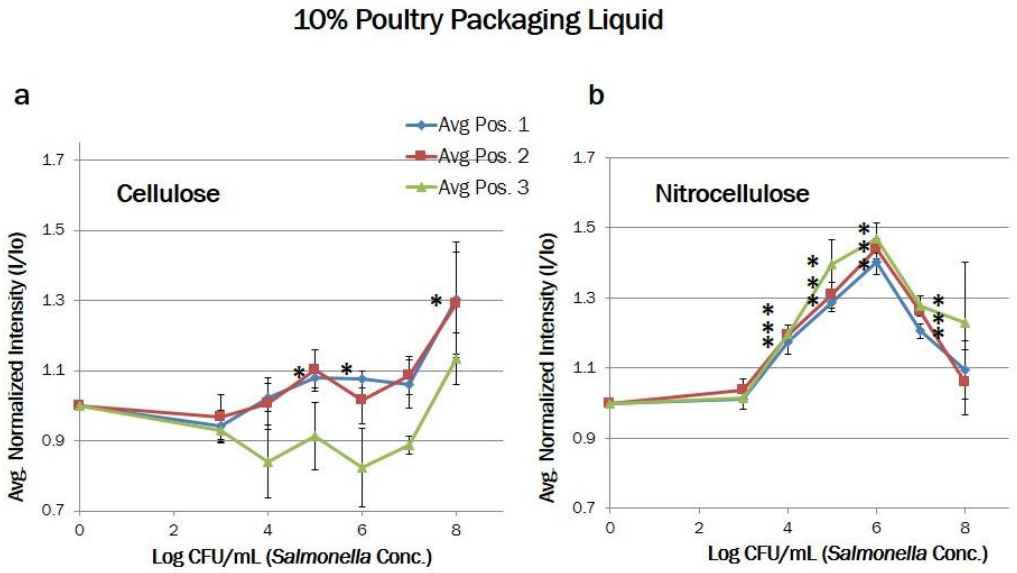

Figure 4: Fluorescent backscattering intensities from DNA extracted from *Salmonella* spiked in 10% poultry packaging on **(a)** cellulose and **(b)** nitrocellulose paper chips. Samples were normalized to a 10% poultry packaging liquid (no bacteria present) negative control to create a standard curve (n = 3). Due to clogging from colony formation, unlysed cells, and proteins from the sample matrix, extraction through cellulose was not efficient. However, in the presence of sample matrix, extraction on nitrocellulose was more efficient, likely from albumin and phospholipic components of the cell membranes acting as surfactants, creating more of a path for DNA migration.

Nitrocellulose extraction of clean *Salmonella* and *Salmonella* spiked in 10% poultry packaging liquid yield a detection limit of 10^4 CFU/mL. The dip present in cellulose extraction is not present in nitrocellulose extraction, and optimal detection occurs at zone 3, although there is less variation in the data between the three zones than in cellulose. This lack of dip is due to the fact that the contents of samples do not penetrate and bind strongly into the nitrocellulose fibers nearly as well as they do into the cellulose fibers, and the nucleic acid likely migrates over the paper to the opposite end of the strip due to charge-charge repulsion. While there is still sufficient mixing of sample and lysis buffer, extraction efficiency is reduced due to lack of paper filtration, thus yielding a higher detection limit than in cellulose. The peak intensities were ~1.25 in DI water (Fig. 3b) and ~1.42 in 10% poultry packing liquid, both at 10^6 CFU/mL. Again, the presence of albumin and phospholipids in the poultry packaging liquid can be attributed to this enhanced fluorescence reading, helping to break up colonies and thereby eliminating the clogging as a natural surfactant. All data points reported are in triplicate ($n = 3$), and a series of t-tests were performed between the data sets of each curve for each detection zone (zones 1, 2, and 3), and most points for zones 1 and 2 passed ($p < 0.05$) in cellulose for each sample type, while most points for all three zones passed ($p < 0.05$) in nitrocellulose. In higher concentrations on both cellulose and nitrocellulose paper, particularly 10^8 CFU/mL spiked in poultry packaging liquid, large error bars and poor t-test results stem from very high amounts of bacteria, protein, and colonization. Most data points showed good statistical significance over the negative controls, with [average – 2 × standard error] being greater than 1. In addition, inconsistencies in data resulted from variations in cellulose fiber threads, which is not an occurrence in nitrocellulose paper, helping further to explain why

error bars typically were smaller in the nitrocellulose tests. Because of the dip between 10^5 – 10^7 CFU/mL due to clogging, cellulose channels proved more appropriate for measuring low and high concentrations of pathogen DNA. Above and below this concentration range, there is a good increase in fluorescence, but this dip may be problematic in obtaining a consistent reading. By contrast, there is no dip between 10^5 – 10^7 CFU/mL in nitrocellulose paper. The most consistent increase in fluorescence appears between 10^4 – 10^6 CFU/mL, making nitrocellulose better for analyzing the mid-range concentrations.

Smartphone direct detection

Direct detection experiments were repeated on cellulose (Fig. 5) and nitrocellulose (fig. 6) paper chips using *Salmonella* at three different concentrations spiked in 10% poultry packaging liquid, and fluorescent was captured using a smartphone (iPhone 4) attached with a fluorescent microscope developed in our lab. The fluorescent signal at the optimized zone 2 region was captured through the miniscope with the CMOS image detector of a smartphone, and pixel intensity was analyzed on ImageJ software (U.S. National Institutes of Health). A standard curve was constructed (averages from three different experiments), normalized to the same negative control, and the data closely corresponds to the data collected using the positioning stage (Figs. 5 and 6). A series of t-tests were performed, and the results showed good statistical significance ($p < 0.05$), with a detection limit of 10^3 CFU/mL. Similar to the other data observed on cellulose, a dip appeared at the expected 10^6 CFU/mL, which is due to clogging prior to zone 1 region on the chip. However, there was a good increase in normalized data over the concentrations of interest, and the data showed good statistical significance over the negative controls, with [average – 2 × standard error] being greater than 1. The total assay time remained 5

minutes. *Salmonella* (10^5 CFU/mL) in 10% whole blood and 10% fecal matter were also extracted in both paper types and detected using the microscope. Signals were normalized to their own negative controls. A series of t-tests were run, and these points showed a good statistical significance over the negative controls, indicating successful DNA extraction. All three data shown in Fig. 5b and 6b show no significant difference, indicating the extraction efficiencies are similar over three different sample matrices.

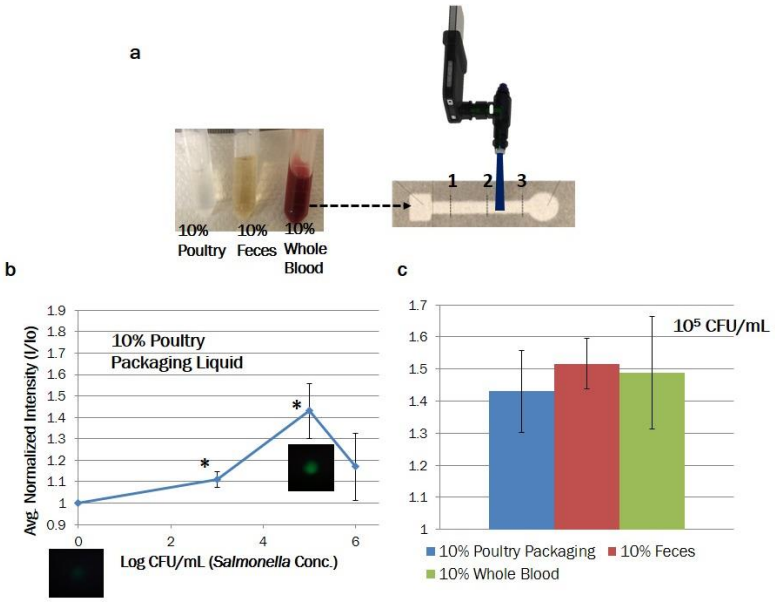

Figure 5: Fluorescent reflectance intensities, taken with an iPhone 4 miniscope **(a)**, from *Salmonella* DNA extracted in cellulose from 10% poultry packaging **(b)**. For comparison, *Salmonella* at a fixed concentration (10^5 CFU/mL) was extracted from three different samples: 1) 10% poultry packaging liquid, 2) 10% whole blood, and 3) 10% feces **(c)**. Poultry packaging samples were normalized to a negative control (no bacteria present) to create a standard curve (n = 3). Blood and fecal samples were also normalized to their own negative controls, and a single point was fit onto the standard curve (n = 3). The phone camera CMOS recorded high definition images of the fluorescence using filters, and a blue LED provided incident light. Images were analyzed on Image J for pixel intensity, and the triplicate intensities were averaged together to create a standard curve.

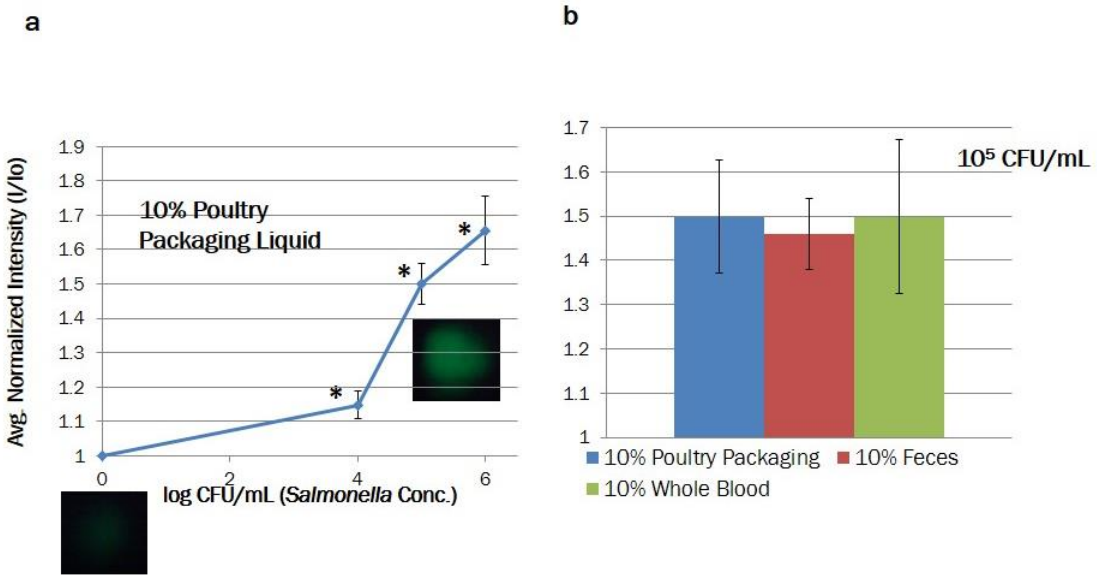

Figure 6: Fluorescent reflectance intensities, taken with an iPhone 4 and miniscope, from *Salmonella* DNA extracted in nitrocellulose from 10% poultry packaging **(a)**. For comparison, *Salmonella* at a fixed concentration (10^5 CFU/mL) was extracted from three different samples: 1) 10% poultry packaging liquid, 2) 10% whole blood, and 3) 10% feces **(b)**. Poultry packaging samples were normalized to a negative control (no bacteria present) to create a standard curve (n = 3). Blood and fecal samples were also normalized to their own negative controls, and a single point was fit onto the standard curve (n = 3). The phone camera CMOS recorded high definition images of the fluorescence using filters, and a blue LED provided incident light. Images were analyzed on Image J software for pixel intensity, and the triplicate intensities were averaged together to create a standard curve.

Smartphone testing with multiplexed chip

In order to ensure a true negative control, and to provide testing feedback, a multiplexed chip was fabricated. The chip was fabricated and assembled (Fig. 7). The chip contained four separate channels: two cellulose and two nitrocellulose, one each for negative controls and one each for testing. This multiplexed chip was tested for extraction

efficiency in *Salmonella* spiked in 10% poultry packaging liquid, and intercalating dye was loaded to determine fluorescent reflectance intensity using an iPhone 4. This chip allows the tester to analyze a given sample at low, medium, and high concentrations of pathogen DNA simultaneously.

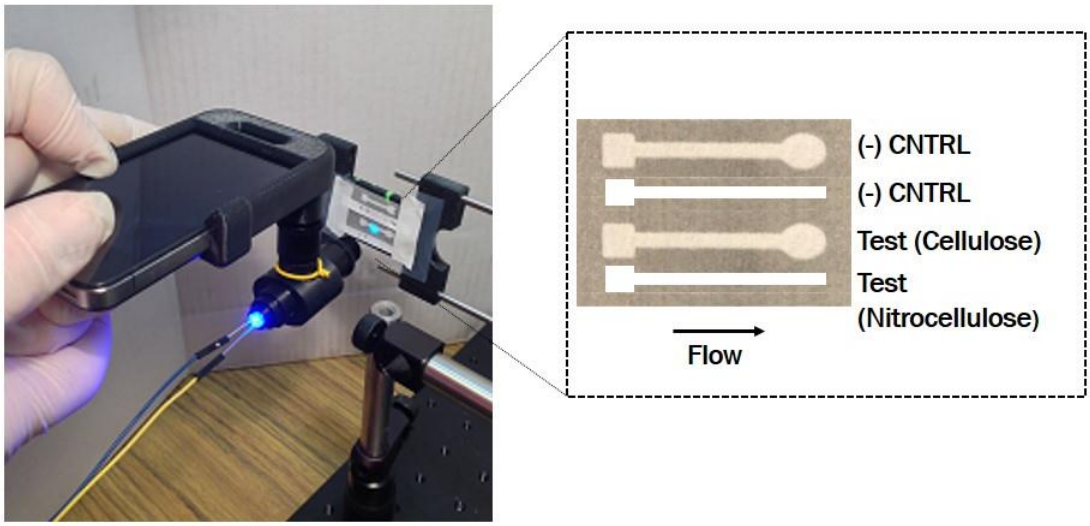

Figure 7: Composite chip, consisting of four separate channels, including negative controls. Cannels alternate between cellulose and nitrocellulose. The chip is dipped into a sample in order to run multiple tests. Shown with iPhone miniature fluorescent microscope. **Note**: Data collected on individual channels.

We have created a sensitive, portable, low-cost device that provides a user-friendly method of extracting total bacterial genomic nucleic acid on a paper microfluidic format. Using fluorescence from Qubit intercalating dye, *Salmonella* Typhimurium Z005 in poultry packaging liquid was quantified in cellulose and nitrocellulose paper chips in two formats: benchtop spectrophotometer system and miniscope. The assay was then shown to work well with conventional PCR. This platform, along with the smartphone apparatus,

will detail an accurate total bacterial count in a real sample while providing the flexibility of interfacing with PCR. This assay is more rapid than the gold standards and can be accomplished in-field in 5 minutes, and it is deposable due to the low cost of fabrication. The assay is sensitive and has a limit of detection well below the infectious dose of *Salmonella*. Cellulose channels proved more appropriate for measuring low and high concentrations of pathogen DNA, while nitrocellulose proved better for analyzing the mid-range concentrations. The presence of three different relevant sample matrices did not impact the accuracy or reproducibility of the scattering intensity signal, nor does it affect PCR. This test has the potential to impact diagnostic worldwide due to its low cost, portability, and ability to interface with a smartphone. In the future, our system can be multiplexed by providing multiple channels on the paper chip for multiple tests, and an element of specificity can be implemented for sorting either DNA varieties or pathogen varieties to create a true field-deployable total analysis system. This system has the potential to have a major impact on the food and medical industries by enhancing field-deployable testing and point-of-care diagnostics and can save these industries millions of dollars by preventing the needless outbreak of common diseases.

Acknowledgements

The authors disclosed receipt of the following financial support for the research, authorship, and/or publication of this article: Funding for this work was provided by Animal and Plant Quarantine Agency, South Korea

References

A. W. Martinez, S. T. Phillips, E. Carrilho, S. W. Thomas III, H. Sindi, and G. M. Whitesides. Simple Telemedicine for Developing Regions: Camera Phones and Paper-Based Microfluidic Devices for Real-Time, Off-Site Diagnosis, Anal. Chem., 80, 3699 (2008).

Centers for Disease Control and Prevention, Trends in Foodborne Illness in the United States, 2012. Last Modified April 18, 2013. http://www.cdc.gov/Features/dsFoodNet2012/index.html.

C.-M. Cheng, A. W. Martinez, J. Gong, C. R. Mace, S. T. Phillips, E. Carrilho, K. A. Mirica, and G. M. Whitesides, Paper-Based ELISA, Angew. Chem., Int. Ed, 122, 4881 (2010).

D. Jonas, M. Speck, F.D. Daschner, and H. Grundmann, Rapid PCR-Based Identification of Methicillin-Resistant Staphylococcus aureus from Screening Swabs , Journal of Clinical Microbiology, 40, 1821-1823 (2002).

D.J. You, P.L. Tran, H.J. Kwon, D. Patel, and J.Y. Yoon, Very quick reverse transcription polymerase chain reaction for detecting 2009 H1N1 influenza A using wire-guide droplet manipulations, Faraday Discussion, 149, 159-170 (2011).

D.J. You, T.S. Park, and J.Y. Yoon. Cell-Phone-Based Measurement of TSH Using Mie Scatter Optimized Lateral Flow Assays, Biosensors and Bioelectronics, 40(1), 180-185 (2013).

D.K. Harshman, R.R., T.S. Park, D.J. You, J-Y Song, and J-Y Yoon. Enhanced Nucleic Acid Amplification with Blood in Situ by Wire-Guided Droplet Manipulation (WDM), Biosensors and Bioelectronics, 53, 167-174 (2014).

E. Carrilho, A. W. Martinez, and G. M. Whitesides. Understanding Wax Printing: A Simple Micropatterning Process for Paper-Based Microfluidics, Anal. Chem., 81, 7091 (2009).

F. C. Huang, C. S. Liao, and G. B. Lee. An integrated microfluidic chip for DNA/RNA amplification, electrophoresis separation and on-line optical detection, Electrophoresis,

27, 3297–3305 (2006).

H. Zhu, I. Sencan, J. Wong, S. Dimitrov, D. Tseng, K. Nagashima and A. Ozcan. Quantum dot enabled detection of Escherichia coli using a cell-phone, Lab Chip, 2013, 13, 1282.

J-G Lee, K.H. Cheong, N. Huh, S. Kim, J-W Choi, and C. Ko. Microchip-based one step DNA extraction and real-time PCR in one chamber for rapid pathogen identification, Lab Chip, 6, 886–895 (2000).

J. Mairhofer, K. Roppert, and P. Ertl, P. Microfluidic Systems for Pathogen Sensing: A Review, Sensors, 9(6) *4804-4823 (*2009).

K. Y. Lien, W. C. Lee, H. Y. Lei, and G. B. Lee. Integrated reverse transcription polymerase chain reaction systems for virus detection, Biosens. Bioelectron., 22, 1739–1748 (2007).

M. U. Kopp, A. J. de Mello, and A. Manz, Chemical amplification: continuous-flow PCR on a chip, Science, 280, 1046-1048 (1998).

O. Mudanyali, S. Dimitrov, U. Sikora, S. Padmanabhan, I. Navruz, and A. Ozcan. Integrated rapid-diagnostic-test reader platform on a cellphone, Lab Chip, 12, 2678 (2012).

P.O. Brown, and D. Botstein. Exploring the new world of the genome with DNA microarrays, Nature Genetics, 21, 33-37 (1999).

S-J Lo, S-C Yang, D-J Yao, J-H Chen, W-C Tuc, and C-M Cheng. Molecular-level dengue fever diagnostic devices made out of paper, Lab on a Chip, **13**, 2686-2692 (2013).

S. Takenaka, K. Yamashita, M. Takagi, Y. Uto, and H. Kondo. DNA sensing on a DNA probemodified electrode using ferrocenylnaphthalene diimide as the electrochemically active ligand, Anal. Chem., 72, 1334–1341 (2000).

T. de Lumley-Woodyear, C.N. Campbell, and A. Heller. Direct enzyme-amplified electrical recognition of a 30-base model oligonucleotide, J. Am. Chem. Soc., 118, 5504–5505 (1996).

T. S. Park, W. Li, K. E. McCracken, and J-Y Yoon. Smartphone quantifies Salmonella from paper Microfluidics, Lab on a Chip, 13, 4832-4840 (2013).

T.D. Lawley, D.M. Bouley, Y.E. Hoy, C. Gerke, D.A. Relman, and D.M. Monack. Host transmission of *Salmonella enterica* serovar Typhimurium is controlled by virulence factors and indigenous intestinal microbiota. Infect. Immun, 2008; 76:403–416.

V. Munster, A. Wallensten, B. Olsen, G.F. Rimmelzwaan, A.D.M.E. Osterhaus, and R.A.M. Fouchier, Influenza A Virus Surveillance in Wild Birds, In Avian Influenza: Prevention and Control; Schrijver, R.S., Koch, G., Eds.; Springer: Dordrecht, The Netherlands, 2005; Chapter 4, pp. 25–30.

X. Mao, Y. Ma, A. Zhang, L. Zhang, L. Zeng, and G. Liu. Disposable Nucleic Acid Biosensors Based on Gold Nanoparticle Probes and Lateral Flow Strip, Anal. Chem., 81, 1660–1668 (2009).